UNIVERSITÀ DEGLI STUDI DI TRIESTE

XXXV CICLO DEL DOTTORATO DI RICERCA IN
BIOMEDICINA MOLECOLARE

Borsa MIUR/Ateneo MD/1 cofinanziata dal Dipartimento di Scienze della vita su fondi del Centro di Riferimento Oncologico Istituto nazionale tumori CRO Aviano

STARD3: A new potential therapeutic target in colorectal cancer

Settore scientifico-disciplinare: **BIO/11**

DOTTORANDO
SALVATORE PARISI

COORDINATORE
PROF. GERMANA MERONI

SUPERVISORE DI TESI
PROF. FLAVIO RIZZOLIO

CO-SUPERVISORE DI TESI
PROF. GABRIELE GRASSI

ANNO ACCADEMICO 2021/2022

Sommario

Introduction

Colorectal cancer (CRC) is the third leading cause of cancer death among men and women worldwide, with a prevalence of more than a million and half cases every year (GLOBOCAN 2020). Although earlier diagnosis (screening, colonoscopy) have contributed to prolong survival in the curable stage of CRC, relatively 25% of patients present metastases at initial diagnosis and approximately 50% will develop metastases, concurring to the high mortality with overall five years survival rate less than 10% for stage IV[1].

Colorectal cancer (CRC) represents a heterogeneous entity, with only a fraction of the tumours responding to available therapies, requiring a better molecular understanding of the disease in precision oncology [2] .

The backbone of first-line treatment in CRC involves traditional systemic chemotherapy drugs (5-FU, oxaliplatin and irinotecan) associated with molecularly targeted treatments based on RAS mutations (Bevacizumab for RAS mutant CRC, Cetuximab or Panitumumab for RAS wild-type CRC) and microsatellite status (pembrolizumab or nivolumab for microsatellite instability-High or deficient DNA mismatch repair CRC)

In the past decade, several efforts have been made to classify colorectal cancers based on location, histology and molecular mechanisms of tumorigenesis for improving clinical management and better predict patient outcome. Despite these therapeutic improvements, only a fraction of the tumours responding to available therapies, including combination therapies, requiring a better molecular understanding of the disease in precision oncology. Nevertheless, chemotherapy is associated with certain limitations, such as existing systemic toxicity, unsatisfying response rate, unpredictable innate and acquired resistance. The estimated deaths in 2021 from colorectal cancer are approximately 900,000 worldwide. There is a crucial need for new diagnostic and therapeutic biomarkers to reduce CRC-related deaths[3].

Pathogenetic mechanism of colorectal cancer

Colorectal tumorigenesis requires a tumour-initiating event, so called driver mutation, that transforms normal intestinal epithelial cells. This event could be a specific point mutation, chromosome rearrangement or copy number variation that alter gene expression[4].

Accumulation of a few subsequential mutations is sufficient for the oncogenic transformation of normal epithelial cells. This process is known as "adenoma-carcinoma sequence" and it is the well-established paradigm for the tumorigenesis of colorectal cancer.

Although colorectal tumours are heterogenous at a genetic level, adenoma-carcinoma sequence proceeds via three main genetic pathways: chromosomal instability (CIN), microsatellite instability (MSI), or through the serrated neoplasia pathway. Chromosome instability is described in 70% to 80% of sporadic colorectal tumours. Microsatellite instability is described in nearly 15% of sporadic colorectal tumors and nearly all colorectal tumors in Lynch syndrome; these tumors are hypermutated and colorectal cancer develops within one to three years and lastly serrated polyps give rise to an estimated 15% of colorectal cancers; some of these tumors are characterized by microsatellite instability and progress rapidly.

Most colorectal tumors arise from pre-cancerous polyps that are broadly categorized as either traditional tubular adenomas or serrated polyps. Mutations in the tumor suppressor *Adenomatous Polyposis Coli* gene (APC) or the B-RAF oncogene are initiating events that give rise to classic adenomas or serrated polyps. These mutations correspond respectively to "first hit" of chromosomal instability and serrated neoplasia pathway, or in other term, the first driver mutation of the "adenoma-carcinoma sequence" [5]. The subsequent events depend on the path that has been taken. As mentioned above, tumorigenesis is characterized by the accumulation of subsequential mutation in specific genes, often corresponding with specific tumors stages. However, not all adenomas progress to cancer: the accumulation of specific mutations in a particular order is essential for progression to malignancy. Moreover, the timeline is pathway

specific: CIN pathway tumorigenesis can take ten years or more, on the other side tumor development via the serrated pathway and comparatively accelerated MSI pathway can occur in a few years[5].

Chromosomal instability (CIN) Pathway

Chromosomal instability pathway is the most common, occurring in 70-80% of cases of colorectal cancer and it is characterized by aneuploidy or structural chromosomal abnormalities, frequent loss of heterozygosity at tumor suppressor gene loci, and chromosomal rearrangements. Colorectal cancer begins as a benign adenomatous intestinal polyp, which develop to advanced adenoma with high-grade dysplasia, and later invasive tumors with metastasis. It has been demonstrated each step is associated with specific genetic alterations in tumor suppressors or oncogenes [6,7].

As mentioned above, the earliest genetic event in CIN pathway is the disruption of APC on 5q21leading to the activation Wnt signaling. Both germline and sporadic mutations in APC have been identified. Germline mutations are responsible for FAP (familial adenomatous polyposis) while somatic mutations are observed in approximately 70%–80% of sporadic colorectal. Germline inactivating mutations are distributed throughout the 5' half of the gene with two hotspots in codon 1061 and 1309, while somatic mutations are clustered in the mutation cluster region (MCR) between codons 1286 and 1513 [8]. Lastly, APC promoter hypermethylation has been also described in 18% of primary colorectal carcinomas and adenomas, representing an alternative mechanism for APC gene inactivation[8]. The APC protein critical function in colon carcinogenesis is its interaction with glycogen synthase kinase-3β (GSK-3β) and β-catenin, regulating the activation of the Wnt pathway—an important pathway for intestinal epithelial cell proliferation. Briefly, in a physiological setting in the absence of a Wnt signal, APC binds and collaborates with GSK-3β and CK1α/ε to phosphorylate β-catenin

leading on its degradation in a proteasome-dependent manner and suppression of the Wnt-signal. While the presence of a Wnt ligand exerts inhibitory effects on GSK3β, phosphorylation of β-catenin no longer occurs, and cytoplasmatic β-catenin can translocate to the nucleus, where the transcription of multiple target genes initiates through displacement of Groucho and the interaction of β-catenin with the T-cell factor (TCF). In mutant APC cells, cells are unable to form the degradation complex and the increased cytoplasmic levels of β-catenin can translocate to the nucleus leading to the constitutive activation of many target genes including oncogene such as cyclinD1, c-myc.

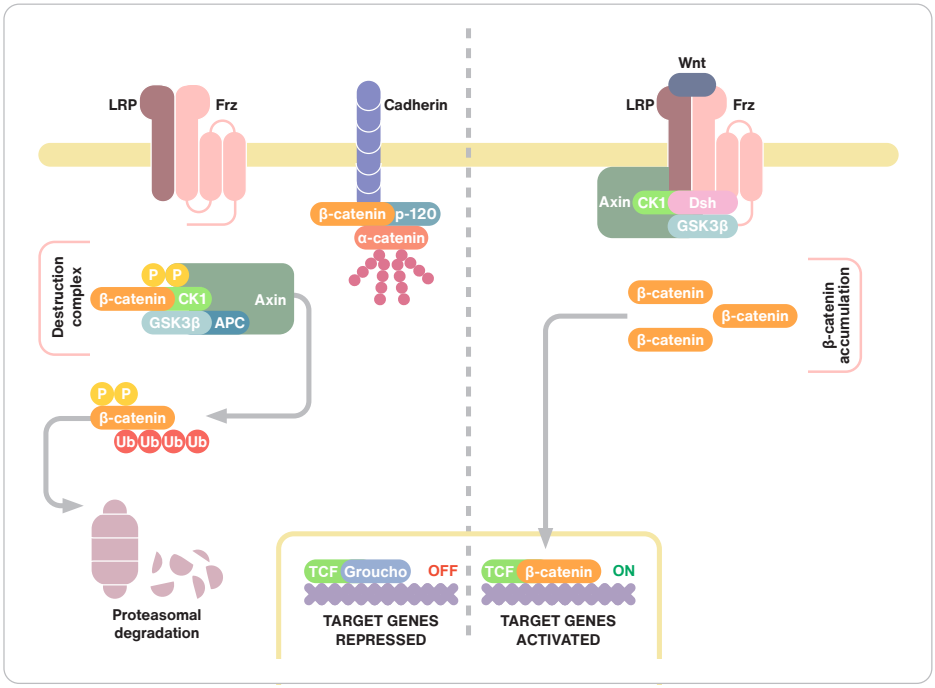

Figure 1 WNT PATHWAY*. in the absence of a Wnt signal, the destruction complex containing adenomatous polyposis coli (APC), glycogen synthase kinase 3β (GSK-3β) and casein kinase 1α/ε (CK1α/ε) targets the degradation of cytoplasmic β-catenin in a proteasome-dependent manner. In the nucleus, Wnt target genes are also kept silent by the repressor Groucho interacting with DNA-bound T cell factor (TCF). In the presence of a Wnt ligand, occupancy of the receptors Frizzled (Frz) and coreceptor low-density lipoprotein receptor-related protein (LRP) triggers the phosphorylation of the cytoplasmic tail of LRP by CK1 and GSK-3β as well as the disheveled (Dsh)-dependent recruitment of axin on phosphorylated LRP. Phosphorylation of β-catenin no longer occurs, and the increased cytoplasmic levels of β-catenin translocate to the nucleus, where the transcription of multiple genes is initiated through displacement of Groucho and the interaction of β-catenin with the T-cell factor (TCF)/lymphoid enhancer factor (LEF) family of transcription factors. (Adapted from Pino, M. S. & Chung, D. C.Gastroenterology 138, 2059–2072 (2010).*

Activating mutations in K-RAS, a component of several growth factor signaling pathways, are the second key event of Chromosomal instability pathway. K-RAS is mutated approximately in 30%–50% of CRCs.[9] Most frequent mutations are single nucleotide point

mutations that occur in codons 12, 13 of exon 2 and codon 61 of exon 3. These mutations block the enzyme in the GTP-bound- activated form, leading to constitutive activation of RAS and the downstream signaling: RAS activates RAF serine-threonine kinases including ARAF, BRAF and CRAF. Activated RAFs activate mitogen-activated protein kinase 1/2 (MEK1 and MEK2), which in turn phosphorylate ERK1 and ERK2. ERK then phosphorylates cytosolic and nuclear substrates, including JUN and ELK1, that regulate enzymes such as Cyclin D1, which is involved in the control of cell cycle progression[4]. As reported in the figure below (Fig.2) , K-RAS also activates phosphoinositide-3 kinase (PI3K) leading to the upregulation of AKT, inducing cell growth, proliferation and survival inactivating pro-apoptotic proteins. K-RAS contribute to colorectal adenoma development but it is described to be not required for adenoma initiation[4].

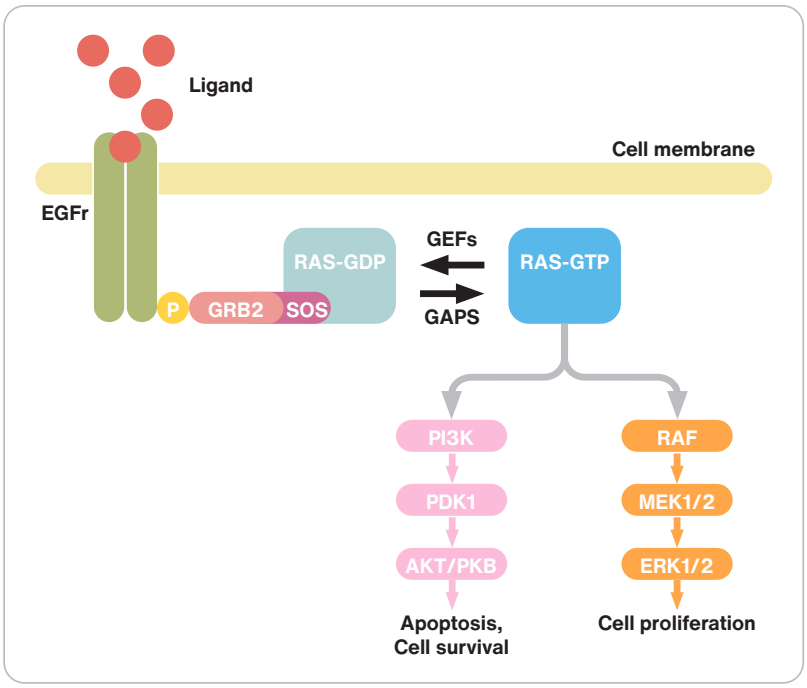

Figure 2 RAS pathway. *Growth factors binding to their cell surface receptors activate guanine exchange factors (GEF) such as SOS (son of sevenless) that are attached by the adaptor protein GRB2 (growth-factor-receptor bound protein 2). SOS stimulates the release of bound GDP from RAS, and it is exchanged for GTP, leading to the active RAS-GTP conformation. The GTPase-activating proteins (GAP) can bind to RAS-GTP and accelerate the conversion of RAS-GTP to RAS-GDP (guanosine diphosphate), which terminates signaling. Mutated RAS is constitutively active in the RAS-GTP conformation. Activated RAS regulates multiple cellular functions through effectors including the Raf-MEK-ERK pathway, PI3K-PDK-AKT pathway. (Adapted from Pino, M. S. & Chung, D. C. Gastroenterology 138, 2059–2072 (2010).*

Another key event in CIN pathway is the harboring of inactivating mutations in the tumour suppressor TP53 gene. TP53 mutations are present in about 60% of CIN tumors[6]. Under certain condition, such as cellular stress, DNA damage, hypoxia, oncogene activation p53 can induce cell cycle arrest, apoptosis, or cell senescence[10]. 74% of TP53 mutation are in the DNA binding domain and they are missense-type mutations with amino acid substitution. These mutations lead to the synthesis of an inactive protein with an abnormally long half-life and not only abrogate the tumor suppressor function, but also novel oncogenic function are acquired, which promote a more aggressive, metastatic cancer phenotype [6,10]. TP53 mutations have been associated with a poor prognosis in colorectal cancer. Mutations are not common in benign colonic adenomatous polyps (15-30%) while mutation rate increases to 80% in advanced colorectal patients with metastases. These findings support the idea that P53 plays a role in the late stage of CIN pathway [6,10].

Loss of heterozygosity (LOH) is defined as the hallmark feature of CIN-positive tumors[8]. In particular, allelic loss at chromosome 18q has been identified in 70% of late stage colorectal tumors and less than 10% of early stage adenoma. It is the final step of adenoma-carcinoma sequence in CIN Pathway. These chromosomal changes lead to a gain and loss of function of tumor-associated genes offering mutated cells growth and survival advantages, starting the progressive conversion of normal cells into cancer cells. However, the gains/losses of chromosomal materials generally span a large region and comprise many genes making identification of target genes challenging. For example, tumor suppressor genes, SMAD2 and SMAD4, localized in 18q21.1, have been proposed as keys element for colorectal cancer progression. SMAD2/4 genes encode downstream signal transducers for transforming growth factor-β (TGF-β), and their alterations could contribute to tumorigenesis. However, the frequency of SMAD2 and SMAD4 somatic mutations is relatively low in CRC. In addition, their gene expression is retained in CRC with LOH of 18q. Taken together, these observations

suggest that SMAD2 and SMAD4 are unlikely to constitute the major chromosome 18q target in CRC[5].

DCC (*deleted in colorectal cancer*) was proposed as another tumor-suppressor gene. It is mapped in the chromosome band 18q21.2. Much of the reported data on the loss and inactivation of DCC is circumstantial and fails to provide conclusive evidence that DCC functions as a tumor-suppressor gene. Furthermore, there are few somatic mutations in DCC reported in CRC and there is no evidence that germline mutations of DCC serve a role in heritable cancer[8].

The insights into the genetic basis of CIN pathway allowed the identification of new prognostic markers and therapeutic target markers (such as monoclonal antibody therapy) in colorectal cancer. CIN is most often linked with poor patient outcome, due to the high intra-tumoral heterogeneity. higher levels of CIN are present in metastatic lesions, compared to non-metastatic colorectal cancers. Finally, CIN has been reported to confer Intrinsic multi-drug resistance (taxanes, doxorubicin etc.) in colon and other types of cancer[11]. Therapeutic target will be discussed in Current therapy in colorectal cancer.

Serrated neoplasia pathway

The serrated pathway is described in 15-30% of all colorectal cancer cases and it is characterized by somatic B-RAF mutation and DNA CpG-Island hypermethylation (CpG island hypermethylator phenotype or CIMP). Basically, activating mutations of the RAS–RAF–MAPK axis initiate and drive the lesion, and CpG island methylation of the promoter regions of tumour suppressor and DNA repair genes lead their neoplastic progression.

Currently, serrated lesions are histologically classified in three subtypes: sessile serrated adenoma/polyp, with or without cytological dysplasia; traditional serrated adenoma (TSA) and hyperplastic polyp (HP).[12] HPs are the most prevalent (60%–75%) serrated lesions, followed by sessile serrated adenoma/polyp (SSA, 20-30%) and traditional serrated adenomas , the rarest subtype accounting for only 1%. On the other side, according to the mutation landscape, the sequence leading to serrated colorectal cancer occurs in two different molecular pathways, the sessile and the traditional serrated routes (Fig,4). Hyperplastic polyps and sessile serrated polyps share some molecular features such as the B-RAF^{V600E} mutation, so some authors considered a subset of hyperplastic polyps as a precursor of sessile serrated polyps[12,13].

B-RAF^{V600E} mutation is the most frequent somatic alteration in the sessile serrated pathway which results in a markedly increased activity of the protein's kinase domain. This causes enhanced signaling through MEK and ERK, a pathway that controls a wide range of tumor-promoting processes, such as cell proliferation and differentiation. Moreover, activating mutations in B-RAF result in widespread methylation of CpG islands. Hypermethylation results in silencing of many genes, such as CDKN2A, which encodes for tumor suppressor p16, insulin-like growth factor binding protein 7 (IGFBP7) and MLH1. Methylation-induced silencing of p16, or as alternative IGFBP7, blocks BRAF-induced senescence and lead to neoplastic progression. The silencing of the MLH1 mismatch repair gene result in high microsatellite instability (MSI-H) and the consequent evolution to colon cancer (BRAF

mutation/CIMP-high/MSI-H). Colorectal carcinomas following the BRAF mutation/CIMP-high/MSI-H pathway make up the majority of sporadic non-syndromic CRCs with MSI-H, accounting for approximately 12-15%[13].

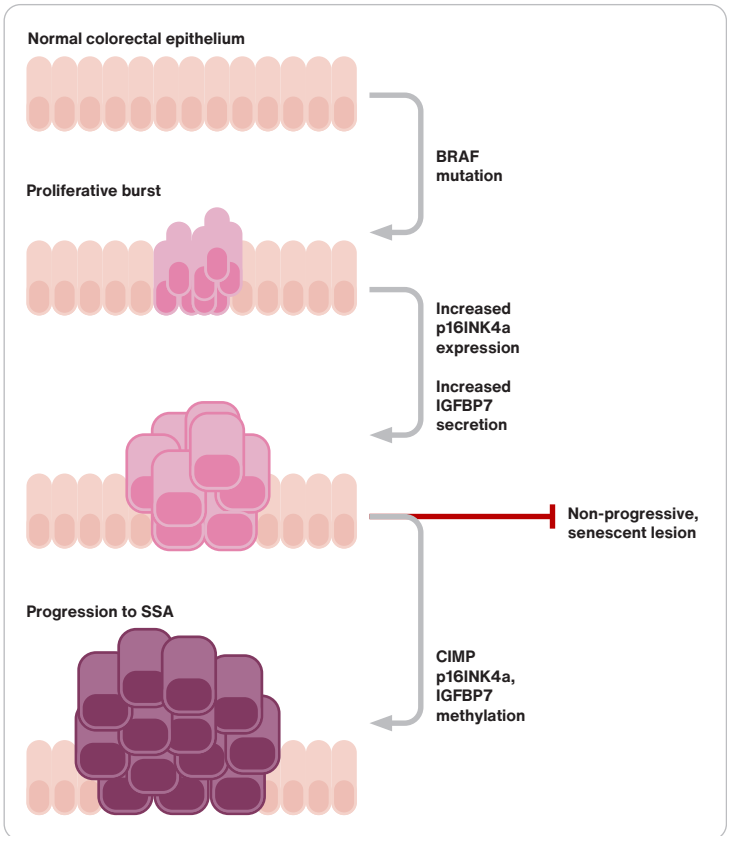

Figure 3 Sessile serrated pathway*.Mitogen-activated protein kinase (MAPK) pathway activation, which results from BRAF mutations, is accompanied by an initial proliferative burst, followed by up-regulation of p16INK4a and increased secretion of insulin-like growth factor binding protein 7 (IGFBP7). Silencing of either p16INK4a or IGFBP7 via methylation in cells with CpG island methylator phenotype (CIMP) could facilitate escape from senescence and progression to sessile serrated adenocarcinomas (SSA). (adapted from Barbara Legget , Vicki Whitehall Gastroenterology 2010 Jun;138(6):2088-100 Role of the serrated pathway in colorectal cancer pathogenesis)*

Traditional serrated pathway has been described as an alternative pathway arising from KRAS point mutation. KRAS acts through the same pathway as B-RAF, so mutations in either protein would have similar functional consequences, supported by the mutual exclusivity of BRAF and KRAS mutations.

However, in comparing tumors that have BRAF mutations with those that have CIMP- high levels, the number of targets that are methylated in tumors with a K-RAS mutation is generally lower. For this reason, the phenotype is referred to as “CIMP-low”[12]. One of the well-described target of K-RAS Methylation-induced silencing is the DNA repair gene methylguanine

methyltransferase (MGMT). MGMT acts removing alkyl groups from the O^6 position of guanine[14] and it has been reported also in hyperplastic polyps and sessile serrated polyps [13,14]. However it is "preferentially associated with KRAS mutations, CIMP-L" in traditional serrated pathway [13,14,15].

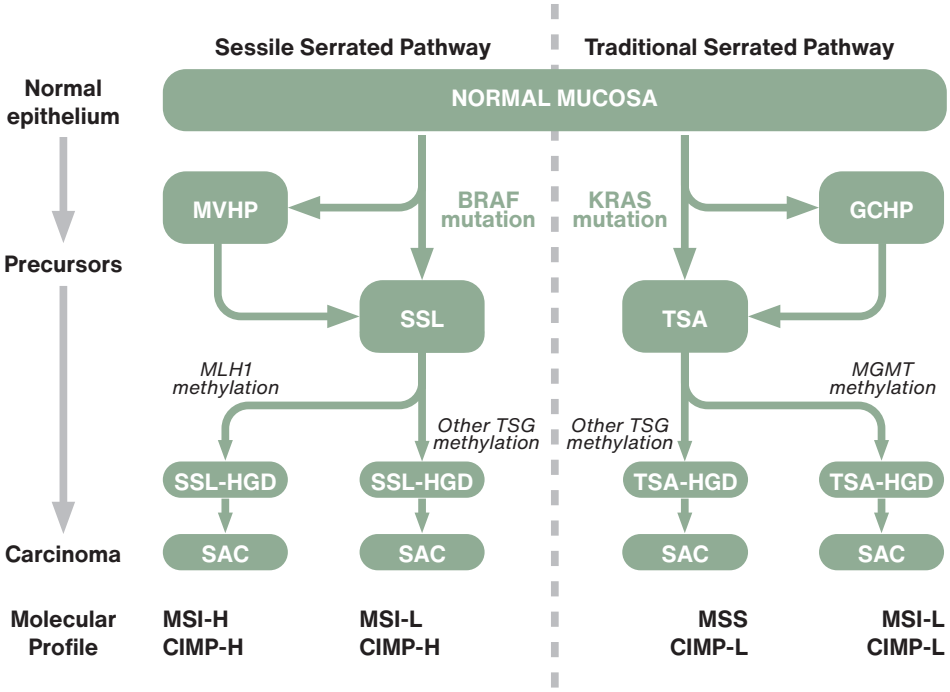

***Figure 4. Serrated neoplasia pathway in colorectal cancer**. (adapted from De Palma, F. D. E. et al. The Molecular Hallmarks of the Serrated Pathway in Colorectal Cancer. Cancers 11, 1017 (2019).*

The end stage of both serrated neoplasia pathways is the serrated adenocarcinoma (SAC). It has been associated more frequently with lymph node metastases (51.8%) than conventional carcinomas (39.9%). It is a histologically well-defined entity with saw-toothed epithelial serrations, abundant clear or eosinophilic cytoplasm, absence of necrosis or < 10% of the total surface area. Sometimes serrated polyp with or without dysplasia can sometimes be seen around its edges[16].

Microsatellite Instability Pathway (MSI)

Microsatellite instability (MSI) or mismatch repair deficient (dMMR) pathway is the third pathway described leading to colorectal cancer (Fig.5). It counts for about 15% of colorectal cancer and it is characterized by widespread instability of short DNA sequences known as microsatellites [17].

MSI result from either mutation of one of the four mismatch repair (MMR) genes, MLH1, MSH2, MSH6, or PMS2, or silencing of the MLH1 promoter by hypermethylation. Physiologically, when in double strands of DNA a nucleotide mismatch occur, these errors are repaired by a MMR enzyme. On the other side, defects in this function result in insertion or deletion (high frequency of replication errors caused by slippage of the DNA polymerase). In cancers with MSI-H, Small insertions/deletions drive to frame-shift mutations within repetitive tracts in the coding region of tumor-suppressor genes and oncogenes. Most frequently, the genes undergoing mutation are: TGF-βR2, Bax, MSH3, ActRIIB, SEC63, AIM2, NADH-ubiquinone oxidoreductase, COBLL1, and EBP1[17,18].

TGF-βR2 poly-adenine tract is the most mutated locus and it is present in approximately 85% of MSI-H CRCs. Frameshifts in these microsatellite sequences inactivate the protein. Moreover frameshift mutations within the polyguanine sequence of BAX gene were described in almost 50% of the MSI-H CRCs, resulting in the inhibition of apoptosis [17]. Lynch syndrome is the hallmark of Microsatellite instability pathway: it is associated with germline mutations in one of the MMR genes; Sporadic MSI tumor are caused by the methylation of MLH1 promoter sequence with an overlapping of molecular and histological features with serrated pathway such as $BRAF^{V600E}$ mutation[19].

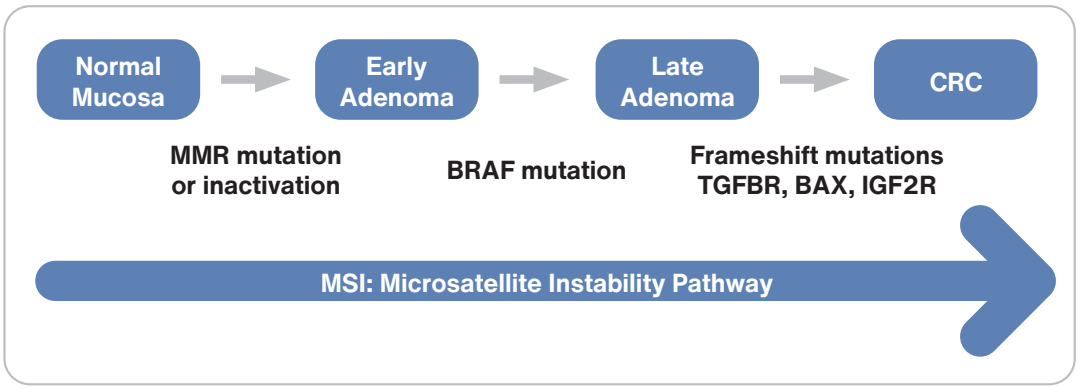

Figure 5 Microsatellite instability pathway *(Adapted from Mezzapesa, M. et al. Serrated Colorectal Lesions: An Up-to-Date Review from Histological Pattern to Molecular Pathogenesis. Int. J. Mol. Sci. 23, 4461 (2022).*

According to the frequency of MSI, tumors can be categorized into three types: microsatellite stable (MSS), low microsatellite instabile (MSI-L), high microsatellite instabile (MSI-H), These cancers tend to arise in proximal colon, to be poorly differentiated, mucinous cell type, and with peritumoral lymphocytic infiltration. [20] Nowadays, microsatellite instability is an important molecular marker for prognosis and adjuvant therapy of CRC [17–19].

Current therapy in colorectal cancer

The following paragraph has been written based on "*NCCN clinical practice guidelines in oncology Colon cancer*" Version 2. 2021 and they are summarized in the figure below (Fig.6).[21]

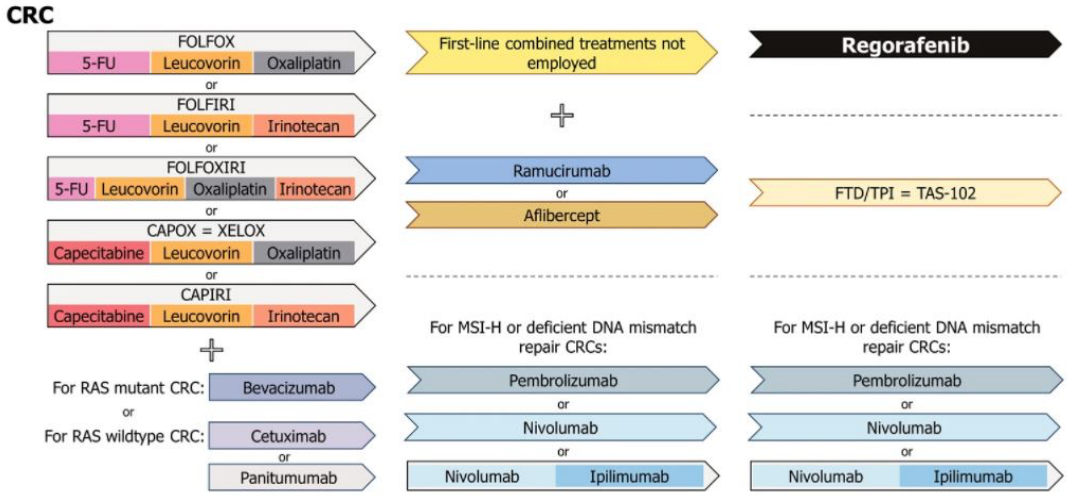

Figure 6 Current therapy in colorectal cancer patients *(adapted from Flavia Fondevila et all: Anti-tumoral activity of single and combined regorafenib treatments in preclinical models of liver and gastrointestinal cancers. Experimental & Molecular Medicine volume 51, pages1–15 (2019)*

The surgical resection is the gold standard for localized non-metastatic stage. There is no evidence for adjuvant chemotherapy for patients with stage I and low-risk stage II. On the other side, Current NCCN guidelines strongly recommend adjuvant therapy for selected stage II with high-risk/pMMR/MSI-S disease and all stage III (node-positive). Current chemotherapy includes both single-agent therapy, which is mainly fluoropyrimidine (5-FU)-based, and multiple-agent regimens containing one or several drugs, including oxaliplatin (OX), irinotecan (IRI), and capecitabine. The combined therapy regimens FOLFOX (5-FU+OX), FOXFIRI (5-FU+IRI), XELOX or CAPOX (CAP+OX), and CAPIRI (CAP+IRI) remain the gold standard in first-line treatment. Randomized phase III clinical trial showed similar efficacy and benefits of CAPOX vs FOLFOX drug combination in metastatic colorectal cancer. Crossover studies and phase III clinical trial showed no significant differences in response rate, progression free

survival (PFS) time and Overall survival (OS) between FOLFOX and FOLFOXIRI. Finally, in meta-analyses similar benefits of CAPOX vs FOLFOX for patients have been described.

Targeted therapy refers to monoclonal antibodies that can inhibit and block molecular pathways critical to cancer-specific growth and maintenance. From 2004 (Food and Drug Administration, FDA, approval of Bevacizumab and Cetuximab) there are several examples of targeted therapy including antibodies against VEGF, the EGFR, B-type RAF (BRAF) V600E, and the human EGFR 2 (HER2). Currently, the therapeutic standard requires also the biological treatment (target therapy) made on presence or absence of KRAS or BRAF mutation. Specifically, anti-EGFR antibodies Cetuximab and Panitumumab in KRAS wild type tumors while Bevacizumab in KRAS or BRAF mutated tumors.

Cetuximab and Panitumumab are monoclonal antibodies targeting EGFR pathway. Panitumumab is a fully human monoclonal antibody while Cetuximab is a chimeric (mouse and human) monoclonal antibody. Cetuximab and Panitumumab are both FDA-approved agents for the first-line treatment. No inferiority or superiority was identified in the phase III ASPECCT study between these two drugs. Patients with known KRAS or NRAS mutations should not be treated with either these monoclonal antibodies, alone or in combination “because they have virtually no chance of benefit”: Cetuximab and panitumumab block the activation of the MAPK pathway. However, the mutated BRAF and KRAS proteins are constitutively active, acting downstream in the EGFR pathway, thus bypassing inhibition of EGFR by Cetuximab or Panitumumab.

A growing body of data has shown that the location of the primary tumor can be both prognostic and predictive of response to EGFR inhibitors: no response was seen in patients with right-sided (cecum to hepatic flexure) primary tumor compared with left-sided (splenic flexure to rectum).

Bevacizumab is a humanized monoclonal antibody that inhibits the activity of VEGF-A. Several clinical trials have demonstrated that adding Bevacizumab to the first lines 5-FU based chemotherapy have improved overall survival of metastatic colorectal cancer patients. However, meta-analysis of randomized clinical trials reported that addition of bevacizumab is associated with a higher incidence of treatment-related mortality than chemotherapy alone (hemorrhage, neutropenia and stomach/intestinal perforation).

Beyond Bevacizumab, three other antiangiogenic agents have been approved for mCRC: Regorafenib, Ramucirumab and Aflibercept. Regorafenib is an oral multi-kinase inhibitor that acts against tyrosine kinases (vascular endothelial growth factor receptor 1 to 3 (VEGFR1-3), platelet-derived growth factor receptor (PDGFR- β), and fibroblast growth factor receptor (FGFR1)) and B-RAF, KIT and RET. The CORRECT phase III trial showed that treatment with regorafenib conferred a significant improvement in OS and PFS compared with the placebo arm, for mCRC that was refractory to standard therapy. Based on this trial, regorafenib has been approved by the FDA in 2012 for the treatment of mCRC patients who have been treated previously with fluoropyrimidine-, oxaliplatin- and irinotecan-based chemotherapy, an anti-VEGF therapy, and an anti-EGFR therapy if KRAS wild type, despite several grade 3 side effects have been reported such as hand-foot skin reaction, hypertension, and rash/desquamation.

Ramucirumab is a monoclonal human antibody that has a high affinity to the extracellular domain VEGFR-2, the essential receptor of the VEGF angiogenic signaling pathway. In patients whose disease progressed on first-line therapy with 5-FU/OXA plus bevacizumab, The RAISE phase III clinical trial has found ramucirumab plus FOLFIRI as second-line treatment of mCRC improved significantly OS and PFS compared with FOLFIRI plus placebo. Based on these results, ramucirumab in combination with FOLFIRI has been approved by the FDA as a second-line option for mCRC in 2015.

Aflibercept is a recombinant fusion protein that can bind to VEGF-A, VEGF-B. It acts as a soluble decoy receptor, preventing activation of VEGF receptors inhibiting the VEGF pathway. In the VELOUR study, aflibercept plus FOLFIRI demonstrated significant improvements in OS and PFS compared with placebo plus FOLFIRI in previously treated mCRC patients. On the other side, the addition of aflibercept to FOLFIRI in first-line therapy had no benefit and increased toxicity (AFFIRM clinical trial's results). The profile of adverse events was similar to that previously reported with bevacizumab, but some adverse events associated with cytotoxic agents were reported at a higher incidence in the aflibercept arm.

Lastly, one of the greatest innovations in terms of the cancer therapeutic revolution has been brought by immunotherapy. However, compared to the other solid tumors, in colorectal cancer less susceptibility to immune checkpoints inhibitor has been reported in clinical trial: the immunotherapy approach with anti-PD1/PD-L1 antibodies (Pembrolizumab and Nivolumab) has demonstrated efficacy only in patients' deficient mismatch-repair mechanism and MSI-high (dMMR/MSI-H, 10-15% of patients). Mismatch repair-proficient (pMMR) colorectal tumor cells express weak immunogenicity and infiltrate a limited number of immune cells, which makes it difficult to induce an adequate immune response and activation.

In conclusion, although the recent advances in the management of colorectal cancer, metastatic disease remains challenging, and patients are rarely cured. For this reason, a better understanding of the pathways implicated in the evolution and proliferation of cancer cells is needed. In this scenario, cholesterol and its metabolites have received increasing attention due to its role in cancer development. Several studies indicate that target-therapies with action directed against cholesterol pathways are promising therapeutic approaches to treat tumour, including colon cancer. Therefore, new cholesterol metabolic targets and drugs for blocking cholesterol biosynthesis and uptake need to be further explored[22].

The role of intracellular cholesterol in cancer

In last years, several target therapy agents, both small molecules and antibodies, have been approved by the FDA used to target the proteasome[22], programmed death-1 (PD-1)/programmed death-ligand 1 (PD-L1) [23], epidermal growth factor receptor (EGFR) [24], cyclin-dependent kinases (CDKs) [25], vascular endothelial growth factor (VEGF)[26] and poly (ADP-ribose) polymerase (PARP) [27,28]. Among novel molecular targets, cholesterol metabolism has received increasing attention due to its role in cancer development [29,30]. In fact, several studies indicated the association between cholesterol levels and cancer development [29]. As an example, serum cholesterol is correlated with an increased risk of more than 10% in prostate cancer recurrence [31,32], and other types of cancer including colorectal [33 34], lung [35,36] and breast cancers [37,38]. On the other side, the use of statin, a class of cholesterol-lowering drugs, is associated with the reduction risk of melanoma, non-Hodgkin lymphoma, endometrial and breast cancers [39,40]. As it concerns colorectal cancer, another study described a dose-dependent reduction in colorectal cancer mortality linked with cholesterol-lowering drugs administration [41].

Recent findings showed intracellular cholesterol levels in cancer cells could be more important than dietary cholesterol in cancer development [42]. Several oncogenic pathway and proteins involved in cancer progression, cell invasion, and metastasis have been associated with intracellular cholesterol [29,43]: the activation of cholesterol synthesis through AKT/mTORC1/SREBP axis (Protein kinase B /mammalian target of rapamycin complex 1/sterol and regulatory element-binding protein pathway) contributed to tumor cell growth[29,44]. In prostate cancer, upregulation of the intracellular cholesterol levels mediated by the AKT pathway promoted cancer aggressiveness and bone metastases [45,46]. Additionally, the activation of aberrant p53-mediated cholesterol synthesis induces the proliferation of breast cancer cells via prenylation of Rho GTPase proteins[42].

Cholesterol can directly activate oncogenic signaling. Cholesterol binds the Smoothened receptor activating the oncogenic Hedgehog signaling pathway leading to cell differentiation, cell proliferation and tumor formation[47]. In addition, cholesterol interacts with PDZ domains of scaffold proteins, such as the N-terminal PDZ domain of NHERF1/EBP50. After NHERF1-cholesterol binding, the signal complex can be activated. NHERF1/EBP50 is one of the major controller of oncogenic signaling networks by assembling cancer-related proteins, including the PI3K/Akt and Wnt/β-catenin pathways [48]. The activation of the PI3K/Akt and Wnt/β-catenin pathways has been found in several types of cancer including colon cancer.

Cholesterol is one of the principal components of mammalian cells and constitutes approximately 30% of the plasma membrane [49]. Physiologically, cholesterol is synthesized in the liver and transported by low-density lipoprotein (LDL) to target cells throughout the body[50]. The cholesterol uptake is mediated by membrane receptors, including LDL receptors such as receptor-related proteins (LRP1, LPR2, LRP5, LRP6, and LPR8), and others [51]. Effectively increasing the capacity to endocytose LDL and LDLR overexpression has been reported in pancreatic ductal adenocarcinoma (PDAC), breast cancer, hepatocellular carcinoma (HCC), lung adenocarcinoma, colorectal carcinoma and other types of cancer [52].

After the internalization, cholesterol distribution is driven by vesicular and non-vesicular transport mechanisms [53,54] . LDL/LDLR complex is driven to early endosomes and then targeted to late endosome/lysosomes. Here, cholesteryl esters are hydrolyzed by lysosomal lipase to free cholesterol. Non-vesicular transport mechanism plays an essential role in maintaining the correct distribution of cholesterol between organelles [53], and several proteins, including the STARD3, are involved as described in the next paragraph [55–57].

Published articles indicated cancer cells showed higher levels of intracellular cholesterol compared to normal cells [58,59]. Tumour cells require high amounts of lipids, nucleic acids and

proteins for their survival. Thus, to compensate for these high requirements, cancer cells modify their metabolism. Among metabolic changes, cancer cells increase the *de novo* lipid biosynthesis including cholesterol synthesis [60–62]. It has been reported that several cancer cell types have higher membrane cholesterol levels and are richer in lipid rafts. These sphingolipid-rich membrane microdomains are originated by cholesterol accumulation, which is involved in the cell signaling, progression, and migration of cancer cells [63–65].

Chun Li et al. provided evidence that human breast (MDA-MB-231 and MCF-7) and prostate cancer (LNCaP and PC-3) cell lines had a higher cholesterol level compared to their non-tumorigenic counterparts [66]. In a study of Zhuang et al. the authors indicated that cholesterol, through the formation of lipid rafts, is a mediator of signal transduction processes relevant to prostate cancer cell survival and disease progression both in vivo and in vitro [67]. Moreover, it has been suggested that progressive increases in membrane cholesterol contribute to the expansion of rafts/caveolae, which may potentiate oncogenic pathways. Supporting these evidences, Badana et al. demonstrated that the decrease of cholesterol in plasma membrane is related to anoikis like apoptosis: methyl-β-cyclodextrin, a cholesterol depleting agent, decrease cell proliferation and migration inducing cell death by apoptosis in breast cancer cell lines (MDA-MB468 and MDA-MB231) [68]. Likewise, Raghu et al., demonstrated that lipid raft disruption in several breast cancer cell lines caused a decrease in the migration and cell invasion compared to normal cells [69].

The role of STARD3 in cancer

Several studies indicated the association between cholesterol levels and cancer development[29]. Cellular cholesterol metabolism, including intracellular distribution and synthesis, is highly coordinated and controlled by a complex protein network, such as sterol regulatory element-binding proteins (SREBPs) [70–72], SREBP cleavage-activating protein

(SCAP) [71,73], 3-hydroxy-3-methylglutaryl coenzyme A reductase (HMG-CoA reductase) [72], insulin induced-genes [73], cytosolic sterol carrier protein 2 (SCP2), fatty acid binding protein (FABP) transfer sterols [72,74], oxysterol binding proteins (OSBPs) [75], protein aster-A (GRAMD1)[76], late endosomal oxysterol-binding protein homologue (ORP1L) [77], Niemann Pick type-C1 and C2 proteins (NPC1 and NPC2)[78], and Steroidogenic acute regulatory (StAR) related lipid transfer proteins (START) [72,79]. These proteins are involved in the vesicular traffic of cholesterol through the endocytic and secretory pathways as well as in non-vesicular exchange between organelles [72,79]. Presently, non-vesicular cholesterol transport has increased its prominence in researchers' community due to the possible correlation between lipid transfer proteins (LTP) and cancer development[72]. For example, latest studies support the idea that cancer cells reprogram cholesterol metabolism to regulate the permeability and fluidity of the cell membrane and increase the transduction of intracellular survival signals [63–65]. Moreover, an increase in the expression of some START proteins has also been associated with cancer cell proliferation, metastases, and resistance to chemotherapy[29,56,80] .

START proteins are a family of LTPs involved in different cellular processes including non-vesicular cholesterol transport [56]. The START family is formed by 15 members divided into six subfamilies according to the similarity of the amino acid sequence and ligand binding [56,81]. Between them, StAR-related lipid transfer domain-3 (STARD3) regulates the cholesterol accumulation in endosomes and mediates its inter-organelle distribution and there are different studies suggesting that STARD3 is associated with several cancer types [82–85].

STARD3 (or MLN64, metastatic lymph node 64) is a transmembrane protein involved in cholesterol transfer and it is localized in the late endosome. STARD3 can also induce the movement of lysosomal cholesterol into the mitochondria stimulating steroidogenesis [86–88] . Several studies indicated that high levels of mitochondrial cholesterol could inhibit apoptotic cell death in different cancer types, in turn inducing tumor progression [83,89].

STARD3 is mapped in 17q12-21 close to the amplicon of the epidermal growth factor receptor 2 (HER2, ERBB2). The amplification/overexpression of STARD3 in cancer suggests that this protein could promote intraneoplastic autonomous steroidogenesis and contribute primarily to the development of steroid hormone-driven cancers, such as breast and prostate cancer [84,85,90].

STARD3 is co-amplified and highly expressed in 25% cases of breast carcinoma [52]. It was demonstrated that several genes, including STARD3, could functionally contribute to the proliferation of cancer cells that present amplification of HER2 [91]. Moreover, high STARD3 levels have been correlated with poor overall survival, disease metastasis-free survival and relapse-free survival in HER2-positive breast cancer and a lower response to trastuzumab therapy [52 92].

Vassilev et al. described in the subpopulation of breast cancer with STARD3 overexpression an increase of cholesterol biosynthesis and Src-kinase activity that may contribute to aggressiveness by increasing membrane cholesterol and enhancing oncogenic signaling [83]. Indeed, co-amplification of STARD3 and HER2 genes contributes to proliferation and metastasis of breast cancer cells by increasing the membrane cholesterol and thereby improving oncogenic signaling [83,91].

Expression profile of STARD3 in breast cancer was performed by Fararjeh and colleagues [92] Using Oncomine database to compare the expression of STARD3 in normal and cancer breast tissues in three different dataset (Guck, Curtis and TCGA). They have found STARD3 significantly overexpressed in invasive breast carcinoma and ductal breast carcinoma *in situ* compared to normal breast tissue. Dissimilarly, down-regulation of STARD3 has been demonstrated in triple-negative breast cancer [93].

Yun et al. described PPP1R1B-STARD3 fusion transcript was found in 21.7% of primary human gastric cancers but not in adjacent matched normal gastric tissues[94]. To support

this finding, *in vitro* experiments on MKN-28 cell lines demonstrated that the expression of fusion transcript PPP1R1B-STARD3 significantly increased cell proliferation and colony formation cell capacity. This increased proliferation was driven by the activation of phosphatidylinositol-3-kinase (PI3K)/AKT axis. Furthermore, *in vivo* experiments on athymic nude mice bearing MKN-28 tumors, PPP1R1B-STARD3 enhanced the tumor growth.

Qiu et al. found a higher expression of STARD3 in tubular and papillary adenocarcinoma compared to poorly differentiated adenocarcinoma cells. It was speculated that this data could be related to the abundance of mitochondria in tubular and papillary adenocarcinoma cells [95].

In prostate cancer, researchers described a linear correlation between the expression of STARD3 and CYP17, an enzyme involved in the steroid biosynthesis pathway[84]. Researchers hypothesized STARD3 and CYP17 expression in prostate cancer could lead to steroidogenesis through constant cholesterol transfer into the mitochondria, increasing the androgen biosynthesis via the catalytic activity of cytochrome CYP17. In this regard, unbalanced expression of STARD3 and CYP17 is associated with a poor prognosis in prostate cancer patients[84].

Altogether, these data show that a high expression of STARD3 may contribute to cancer aggressiveness by cumulating membrane cholesterol. However, the molecular mechanism by which STARD3 is involved in tumor is still elusive. Several authors have postulated its role in cholesterol transport between the ER and endosomes [96]. The integral ER membrane proteins vesicle-associated membrane-protein (VAMP)-associated protein (VAP) is a protein family (VAP-A and VAP-B) found in almost all eukaryotes, which interact with STARD3 [83,96–98]. STARD3 contains non-conventional phenylalanines in an acidic tract protein motif (described by Di Mattia et al as a non-conventional FFAT motif) with seven core residues in an acidic flanking region that contains a serine residue at the 4th position instead of an acidic residue and

it is able to bind VAP proteins and MOSPD2 (Motile sperm domain-containing protein 2) through the interaction with the MSP domain [99] (Fig 7). It was hypothesized that abnormal ER structures called *karmellae* could be produced by ER-endosome interaction in response to STARD3 overexpression inhibiting late endosome maturation in to lysosomes (Fig. 7) [96,100–102]. Under this state, lysosome degradation activity may be compromised : cell surface growth factors receptors, such as HER2, could be not degraded, driving to uncontrolled cell growth, as a consequence of a continuing signal transduction [95]. Along these lines, STARD3 may increase the progression of HER2-positive cancer. This hypothesis is supported by the experimental data obtained by Vassilev and colleagues, who showed that STARD3 overexpression enhances oncogenic signals in breast cancer cell lines [83].

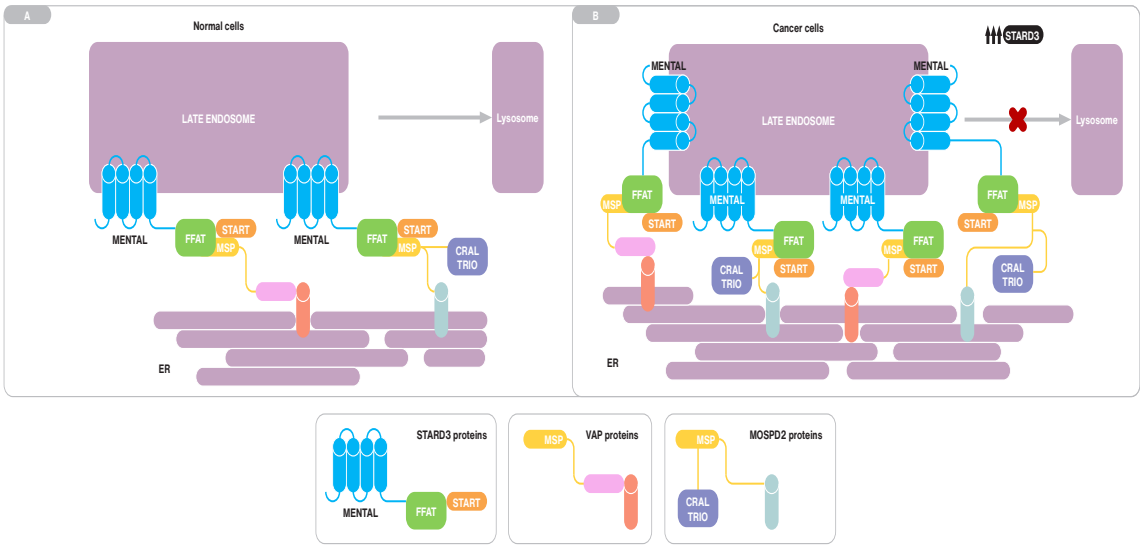

Figure 7 Endoplasmic reticulum-endosome interaction in normal (A) and cancer cells overexpressing STARD3 (B). *START domain interacts with vesicle-associated membrane protein (VAP) or motile sperm domain containing protein 2 (MOSPD2) to form membrane contact site. STARD3 overexpression could inhibit late endosome lysosome maturation (from Asif et al, 2021)*

An additional potential molecular mechanism played by STARD3 during tumorigenesis is through mitochondrial intermembrane trafficking of cholesterol [29,89]. Although mitochondria have low cholesterol level compared to other organelles, cancer cells have higher content of mitochondrial cholesterol that could constrain cell death by inhibiting the release of apoptotic proteins from mitochondria. Some authors supposed that STARD3 could be involved in

cholesterol transport from late endosomes to the ER and subsequently to the mitochondria via the mitochondria-associated ER membrane (MAM) [96,103,104]. Authors indicated that the STARD3-VAP complex induces the formation of membrane contact sites (MCS) [88] (Fig.8). Although the STARD3-MOSPD2 complex does not participate in the formation of ER–mitochondria MCS [105], the association of the ER with both late endosomes and mitochondria through MCSs scaffolded by VAPs may contribute to cholesterol transport [96,104]. To support this hypothesis STARD3 depletion dramatically reduced lysosome-mitochondria MCS in NPC1-deficient cells, indicating the crucial role of STARD3 in the MCS formation and the regulation of cholesterol transport to the mitochondria [87,106].

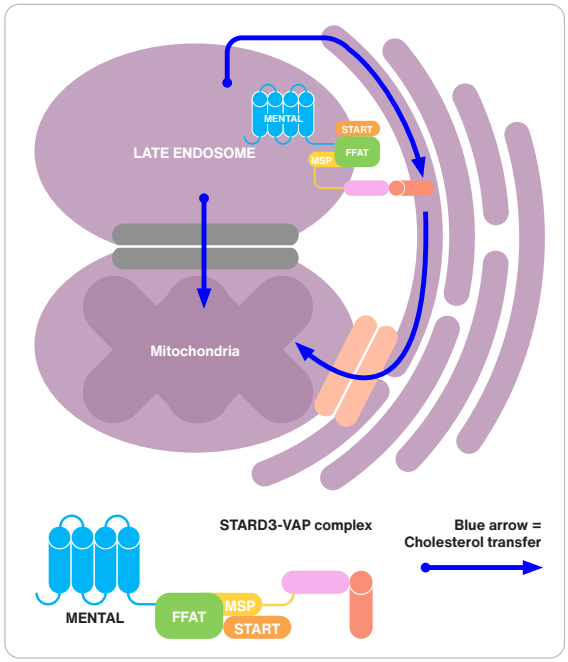

Figure 8 Possible model for cholesterol transport to mitochondria. *ER-LE interaction via the STARD3-VAP complex. Cholesterol is driven to mitochondria via either the ER-mitochondria MCS or MAM (mitochondria-associated ER membrane). Contact between late endosome membranes and mitochondria membrane also allows direct transfer of cholesterol. (from Asif et al, 2021)*

In line with this data, STARD3 could be a molecular target for therapeutic treatments pointed to the cholesterol metabolism in tumour cells. As STARD3 is a cholesterol-specific START protein, the challenge is to switch off the abnormal function or expression of this protein in

cancer cells. Therefore, STARD3 could be a therapeutic target for the successful development of novel molecular therapies.

STARD3 somatic mutation in cancer

COSMIC (Catalog of Somatic Mutations in Cancer) database reveals several STARD3 somatic mutations in several tumor types. COSMIC is an expert- curated database of somatic mutations reported in the scientific literature or from the Cancer Genome Project, exploring the impact of somatic mutations in human cancer. The analysis from COSMIC refers to 38,259 unique samples from patients with different types of cancer including breast, lung, liver, ovary, skin, nervous system, intestinal, and stomach cancer (retrieved on 26 April 2021). The analysis was conducted applying the following filter/criteria: 1) only mutations in tumor samples (not cultured samples) where both tumor and germ-line samples of the same patient have been analyzed and the variant allele is present only in the tumor sample (confirmed somatic mutation) were considered; 2) or no germ-line allele information was available, but the variant has been reported 'Confirmed Somatic' in a normal–tumor sample pair from another patient; 3) only mutations predicted to be pathogenic by the FATHMM algorithm.

Overall, the analysis revealed the existence of 88 somatic mutations affecting STARD3. The results showed that mutations are distributed over the entire length of the protein, with a slight prevalence in the START domain (49%) compared with the MENTAL domain (38.6%). The most frequent mutation is present in residue 117 (R117Q) in 5 patients with adenocarcinoma (3 in the intestine and 2 in the stomach). The same mutation is also reported in thyroid and prostate cancer, but tumor samples are not specified; for this reason, they were not included in the analysis. Only one pathogenic mutation (0.99 predicted score) is present in the FFAT-like motif of the protein. This missense mutation leads to the replacement of the amino acid serine with leucine at position 209 and is present in a dedifferentiated liposarcoma. It has been reported by Di Mattia et al. that the phosphorylation of this serine (4th residue of

the FFAT motif) of STARD3 is necessary for ER–endosome contact formation in vivo and for sterol transfer function in vitro [99]. It is, therefore, possible to hypothesize that when this amino acid is mutated to leucine there is an abrogation of ER–endosome contact sites since it was previously reported that the substitution of the other amino acids of the FFAT-like motif (residue 207 and 208) abrogates ER–endosome contacts [97].

STARD3 Protein structure

The human STARD3 protein is a sterol-binding protein composed of 445 residues. The first 170 ammino acids coincide to the transmembrane portion and it is formed by four helical regions of approximately 20 residues[107] . Regrettably, there is no 3D information in the literature concerning this protein region, nor is it possible to construct a homology model[108]. The only possibility to obtain a 3D model of this protein region would be the development of an ab initio model[109]. The domain that distinguishes STARD3 from the other START domain proteins is called MENTAL (MLN64 NH2-terminal). This domain anchors the protein to late endosome membrane, exposes the START domain in the cytosol, and mediates homotypic as well as heterotypic interactions between STARD3 and its paralog, STARD3NL protein[97]. Already published data show that this domain interacts with cholesterol, suggesting the hypothesis that it acts as sterol reservoir. [110,111]

The region corresponding to the 170-445 sequence constitutes the STARD3 cytoplasmatic domain and it is responsible for binding to cholesterol. Two crystal structures of the apo START at 1.74 Å resolution and 2.2Å have been already published (5I9J [112] and 1EM2 [113] PDB code, respectively). As described in fig. 9, the domain adopts a helix-grip fold with a nine-strand β-sheet and three α-helices, with the cavity entrance guarded by an omega loop (Ω1) that links the β5 and β6 strands.

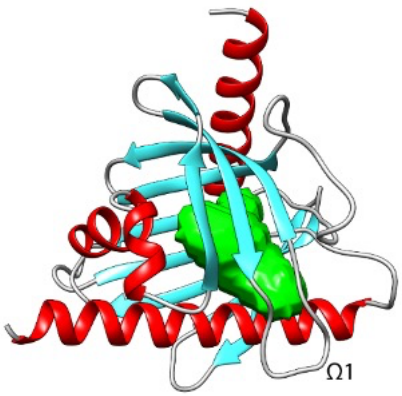

Figure 9 3D structure of STARD3. The cavity of the cholesterol binding pocket is green

An analysis with BLAST software suggested that among the other human proteins, beyond its close paralogue STARD3NL (STARD3 N-terminal like), STARD1 is the one with the highest similarity. It shows 31.6% of conserved residues with respect to STARD3. In addition, the cholesterol molecule located within the STARD1-START binding pocket has a lower degree of freedom than the cholesterol molecule within the STARD3-START pocket, suggesting differences in the orientation of the cholesterol ring within the cavities of each protein[114]. The other STAR proteins show a lower level of similarity; however, as shown in fig.10, a superimposition between the available human STARD1, STARD3, STARD4, STARD5, and STARD6 x-ray structures, highlights the same secondary structure. STARD3 and STARD1 showed identical or highly conserved residues at three positions that could be important for ligand binding: 1) an acidic residue at position 332 (Asp in STARD3 and Glu169 in STARD1), 2) the conserved Gln421 (position 258 in STARD1) and 3) the conserved Arg351 (STARD3 residue numbering), Interestingly, the electron-density maps reported by Horvath and co-workers (5I9J PDB code), highlight two alternative conformations for Arg351; one of which is able to form a salt-bridge with Asp332 that partially occludes the internal cavity of the protein. Based on these observations, the authors hypothesized that this salt-bridge in STARD3 could act as an allosteric trigger point to communicate ligand binding to retinal proteins and enzymes involved with xanthophyll transport and metabolism [112]

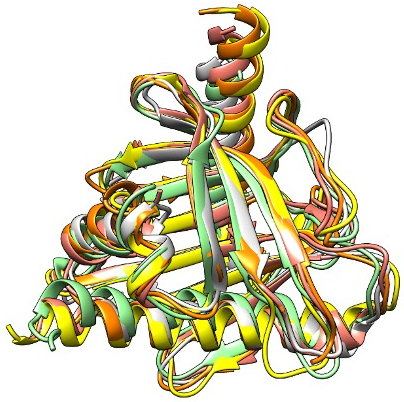

Figure 10 Superimposition between the secondary structure of STARD1 (orange), STARD3 (yellow), STARD4 (white), STARD5 (salmon), and STARD6 (green).

3D *in vitro model* for colon cancer research

The recent advances in in vitro 3D culture technologies, such as organoids, have opened new avenues for the development of novel, more physiological human cancer models. Organoids can be grown from embryonic and adult stem cells and display self-organizing capacities, phenocopying general architecture and functional aspects of the organs of origin[115]. Thanks to that, organoids are becoming essential for a more efficient translation of basic cancer research into translational research, precision medicine and target therapy.

Organoid technology can be utilized to study cancer- related processes and signaling pathways: Normal epithelial (wild-type) organoids can be engineered to study the role of specific mutations in tumorigenesis, in a setting that approaches the physiological environment: two research articles published in parallel demonstrate that it is possible recreate *in vitro* the "adenoma-carcinoma sequence"[116,117]. In Drost authors injected subcutaneously engineered mutant organoid into immunodeficient mice. After 8 weeks, 3 out 12 mice injected with APC knock-out/K-RAS G12D/ /P53 Knock out organoids ('triple') and 13 out of 16 mice injected with APC knock-out/K-RAS G12D/ /P53 Knock out/ SMAD4 Knock out organoids ('quadruple') developed visible tumours. Histological analysis confirmed that triple organoids did engraft but remained small with few proliferating cells and mostly resembled adenomas. Quadruple-derived tumours displayed characteristics of invasive carcinoma, including an irregular multi-layered epithelium consisting of tumour cells with increased nuclear–cytoplasmic ratio, pleiomorphic and hyperchromatic nuclei. Thus, introduction of oncogenic mutations sequence KRAS, APC, P53 and SMAD4 enables normal human intestinal stem cell organoids to grow as tumours with invasive carcinoma features *in vivo*. Moreover, APC knock-out/P53 Knock out in organoids is sufficient to acquire CIN. Similarly, in Matano research

paper engineered organoids (APC knock-out/P53 Knock out/ SMAD4 knock out and $KRAS^{G12V}$ or $PI3KCA^{E545K}$) are able to form tumour under the kidney subcapsule in mice [117]. Additionally, organoids can be grown with a high efficiency from patient-derived healthy and tumour tissues, potentially enabling patient-specific drug testing and the development of individualized treatment regimens. Patient derived organoid (PDO) mimic the primary tissues in both architecture and function and retain the histopathological features, genetic profile, mutational landscape, and even responses to therapy. In 2018 it was demonstrated for the first time patient derived organoid could predict treatment response in cancer patients[118]. In colon cancer, the TUMOROID trials reported PDO drug screening results were associated with the observed clinical response in patients treated with irinotecan- based regiments[119]. The results from growth rate inhibition metric (GR) were predictive for the best RECIST response to irinotecan-based treatment observed in the lesion from which the PDO was obtained. 50% of patients with the most sensitive *in vitro* results had significantly longer progression-free survival (PFS, median 169 versus 58 days). In another trial (CinClare trial), PDO drug screening results (organoids size) were predictive for clinical response (tumour regression grade upon resection) in 80 locally advanced rectal cancer patients receiving neoadjuvant chemoradiation, randomized for capecitabine or capecitabine and irinotecan[118].

These results suggest PDO drug screening results may be predictive in future for clinical response in CRC patients. Currently, there are 17 ongoing clinical trials on patients using organoids as primary or secondary outcome results (review at https://clinicaltrials.gov/ search parameters:" colorectal cancer" and "organoid").

Rank	NCT Number	Title	Status	Outcome Measures
1	NCT05304741	The Culture of Advanced/Recurrent/Metastatic Colorectal Cancer Organoids and Drug Screening	Recruiting	Progression-free Survival|Overall Survival|Diagnostic Indicators
2	NCT05384184	Next Generation " Pre-clinical Model for Colorectal Cancer Metastases and Hepatocellular Carcinomas (BORG)	Recruiting	Build the next generation biobank of liver-derived organoids|Biobank of liver-derived organoids efficiency|Evaluate the clinical relevance of the generated organoids
3	NCT04755907	3D Bioprinted Models for Predicting Chemotherapy Response in Colorectal Cancer With/Without Liver Metastases	Recruiting	Response of 3D tumor models/organoids to the same chemotherapy drugs as the corresponding patients.|Response of the colorectal cancer patients to neoadjuvant chemotherapy.
4	NCT04996355	Organoids-on-a-chip for Colorectal Cancer and in Vitro Screening of Chemotherapeutic Drugs	Recruiting	The accuracy, specificity and sensitivity of organoids-on-chip for drug sreening
5	NCT05183425	Patient-derived Organoids Predicts the Clinical Efficiency of Colorectal Liver Metastasis	Recruiting	The consistency of drug sensitivity|The establishment of PDO
6	NCT05401318	Tailoring Treatment in Colorectal Cancer	Recruiting	Clinical logistics pipeline for patient-derived organoid development success rate|Sensitivity report for chemotherapy and cellular immunotherapy by clinical evaluation|Induction of immunotherapy efficacy by chemotherapy in colorectal cancer, measured by advanced imaging analysis
7	NCT05038358	Tumor Immune Microenvironment Involvement in Colorectal Cancer Chemoresistance Mechanisms	Not yet recruitin	Percentage of viable organoids for 60 days of culture maintenance.
8	NCT04842006	Systemic Neoadjuvant and Adjuvant Control by Precision Medicine in Rectal Cancer	Recruiting	Recurrence-free survival|Postoperative ctDNA|CRC-specific survival|overall survival|number of surgically resected patients resected patients|R0-resection rate|local recurrence rate|complete pathological response response rate|complete clinical response rate|total uptake of chemotherapy|adverse effects of surgery effects of surgery|adverse effects of chemotherapy|Treatment response by patient-derived organoid (PDO) therapy response
9	NCT04279509	Selecting Chemotherapy With High-throughput Drug Screen Assay Using Patient Derived Organoids in Patients With Refractory Solid Tumours (SCORE)	Unknown status	Overall radiological response rate|Correlation between patient genotype, tumor biomarkers and blood biomarkers with clinical outcome
10	NCT04220242	Future of Colorectal Cancer Surgery	Recruiting	Video recordings of Colorectal Cancer.|Analysis of video recordings|Biophysics visualisation software development|Biophysics model training|Validation of predictive accuracy biophysics-visualisation model|Coefficients of Variation|Microscopic Map of intratumoral fluorophore accumulation|Realtime delineation display of tumour area including margins
11	NCT02732860	Personalized Patient Derived Xenograft (pPDX) Modeling to Test Drug Response in Matching Host	Recruiting	Measure of drug sensitive pPDX to a panel of drugs as a predictor of clinical response in matched host|Rate of results reporting|Rate of pPDX engraftment|Comparison of actionable alterations identified in clinical and pPDX samples|Number of patients with molecular abnormalities in pPDX as identified via NGS eliciting clinical responses while receiving matched treatments.|Correlation between pPDX and organoid drug sensitivities
12	NCT04714957	PITCHER (Peritoneal Carcinomatosis Heterogeneity)	Recruiting	genetic and epigenetic data available for 20 "multiplets" biospecimens (peritoneal carcinomatosis + healthy tissue + primary tumor + tissue from other tumor metastasis - when applicable and available-)
13	NCT05412706	Niraparib Maintenance Treatment in mCRC With a Partial o Complete Response After Oxaliplatin-based Induction Therapy	Not yet recruitin	Progression-Free Survival 1|Progression-Free Survival (2) after re-introduction of first-line treatment combination|Overall Survival|Objective Response Rate|Incidence of Treatment-Emergent Adverse Events
14	NCT04587128	Early-Line Anti-EGFR Therapy to Facilitate Retreatment for Select Patients With mCRC	Recruiting	Cohort A Objective Response Rate (ORR)|Cohort B Progression Free Survival (PFS)|Cohort A Progression Free Survival (PFS)|Cohort B Objective Response Rate (ORR)|Type and Severity of Toxicities|Rate of Retreatment with EGFRi|Overall Survival (OS)
15	NCT03146962	High Dose Vitamin C Intravenous Infusion in Patients With Resectable or Metastatic Solid Tumor Malignancies	Recruiting	Change in antitumor activity measured by pathologic response based on tumor regression grading in cohort A patients.|3-month disease control rate (DCR) will be evaluated using RECIST v 1.1 in cohort B patients.|Maximal tolerated dose of high dose vitamin C in combination with Y90 radioembolization|Progression-free survival (PFS)|Objective response rate (ORR)|Assessment of pharmacokinetics of high dose vitamin C plasma levels concentrations|Safety of high dose vitamin C administration using CTCAE 4.03.
16	NCT04622423	Advanced Therapies for Liver Metastases	Recruiting	Definition of tumor mutational burden, epigenetic and gene expression profile of the CRC and PDAC metastatic liver at bulk and at single cell level|Characterization of the immune landscapes of CRC and, if possible, PDAC liver MTS by high dimensional flow cytometry|Histological validation of the molecular results obtained in 1. and 2.|Definition of the antigenic landscape and TCR repertoire of CRC and PDAC liver MTS|Evaluation of the molecular and cellular composition of CRC and, if possible, PDAC liver MTS by spatial transcriptomics technologies (NICHE-seq and Visium)|Collection of clinical follow-up data|Collection and biobanking of follow-up samples from patients with CRC and metachronous PDAC MTS to the liver|Biobanking of biospecimens collected from CRC and PDAC patients and from healthy donors
17	NCT05630794	Testing ONC201 to Prevent Colorectal Cancer	Not yet recruitin	Mean change in human adenoma tumor necrosis factor-related apoptosis-inducing ligand (TRAIL) expression in polyps induced by ONC201|Mean change in normal human mucosa TRAIL expression induced by ONC201|Proportion and severity of treatment emergent adverse events

Table 1 Clinical trial in colorectal cancer using organoids. (Revision 15 December 2022)

Aim of the study

Colorectal cancer (CRC) is the third leading cause of cancer death in Europe, with a prevalence of more than a million cases every year. Primary or acquired resistances to therapies are the major limits to be addressed. The overall five years survival rate is less than 10% for stage IV and only a fraction of the tumours responds to available therapies [1].

In this scenario, cholesterol metabolism has received increasing attention due to its role in cancer development. Cancer cells show higher levels of intracellular cholesterol compared to normal cells. Tumour cells require high amounts of lipids, nucleic acids and proteins for their survival. Cancer cells increase the de novo lipid biosynthesis including cholesterol synthesis [60]. Cellular cholesterol metabolism, including intracellular distribution, is highly coordinated and controlled by a complex protein network. Between them, StAR-related lipid transfer domain-3 (STARD3) regulates the cholesterol accumulation in endosomes and mediates its inter-organelle distribution.

This research project aims to demonstrate STARD3 is a valid therapeutic target for colorectal cancer patients. To the best of our knowledge, there are no other groups aimed at demonstrating STARTD3 as a valid therapeutic target in CRC patients. Up to now, only one STARD3 inhibitor has been developed by our group [82]. The VS1 compound is able to inhibit cholesterol interactions with STARD3 in the low micromolar range. Considering the emerging role of cholesterol metabolism in cancer, the number of publications related to cancer, and the druggability of the protein (cholesterol-binding pocket on the START domain), STARD3 represents a strong candidate as a new therapeutic target as in colorectal cancer.

Materials and methods

Cell culture cell lines

HCT-116, HT-29, Colo-205 and Colo-201 colon cancer cell lines were purchased from the European Collection of Authenticated Cell Cultures (ECACC), HEK293T from American Type Culture Collection (ATCC), NIH3T3 and MRC-5 were kindly donated by Gustavo Baldassarre (National Cancer Institute (CRO) of Aviano).

HCT116 and HT-29 colon cancer cells were grown in T75 flasks in McCoy's 5A medium (Gibco™) supplemented with 10% FBS (Microgerm, RM10432), 100 U/ml Penicillin and 100µg/ml Streptomycin (Euroclone, ECB3001D). Colo-201 and Colo-205 colon cancer cells were grown in in T75 flasks RPMI medium (Gibco™), 10% FBS (Microgerm, RM10432), 100 U/ml Penicillin and 100µg/ml Streptomycin (Euroclone, ECB3001D). NIH3T3 and MRC-5 cells were grown in Dulbecco's modified Eagle's medium (DMEM, Gibco™) supplemented with 10% FBS, Non-Essential amino acids (Lonza) and 100 U/ml Penicillin and 100µg/ml Streptomycin (Euroclone, ECB3001D). HEK293T cell lines was cultured in Iscove modified Eagle's medium (IMDM, Lonza) supplemented with 10% FBS.

Upon reached the confluence of 85-90%, cells were washed twice with PBS (Gibco, 14190144) cells were detached by trypsin 0,05% (Sigma-Aldrich). After trypsin inactivation, cells were resuspended in the appropriate medium and centrifuged 5 minutes at 1000 rpm. The resulting cells pellet was resuspended using fresh medium and the cells counted by Bürker haemocytometer. The cells were seeded accordingly to the experimental condition. All cell lines were cryopreserved for long-time storage in FBS containing 10% DMSO in liquid nitrogen after one week in a Mr. Frosty at -80°C. All the cells were cultured at incubator condition: 95% humidity, 5% CO2, and 37°C. Mycoplasm contamination was checked monthly using MycoAlert® PLUS Mycoplasma Detection Kit (Lonza, LT07-705).

Short hairpin and lentivirus productions

The shRNAs and plasmids were purchased in bacterial glycerol stock format. Each bacterial clone, correspondent to one clone, was streaked on LB agar plate, selected with ampicillin (100µg/ml) and left to grow overnight at 37° C. The resulting colonies were picked up and inoculated in LB medium (Thermo Scientific) and cultured overnight at 37° C in an orbital incubator. The bacterial culture was centrifuged, in order to recover the pellet, at 4500 rpm for 10 min, then the supernatant was discarded. The plasmid DNA was purified from the bacterial pellet by Plasmid Midi Kit (Roche) following manufacturer's instruction. The quantity and quality were assessed by nanodrop (Thermo Fisher Scientific). The plasmids were stored at -20°.

For lentivirus production HEK293T cell line was plated in 6-multiwell. The day after (60%-80% confluency), cells were transfected using a mix of:

-2µg of lentiviral plasmid encoding the gene of interest or shRNA of interest.

- Lentiviral packaging vectors (1µg of PAX2 and 0,5µg of pMD2G).

- FuGENE® HD Transfection Reagent (Promega) according to manufacture instruction.

Supernatant media (containing lentivirus particles) were collected after 48h and 72h. Media were filtered with 0.45µm MILLEX-HP filter, aliquoted and stored at -80°C.

Cell lines transduction

Colon cancer cell lines (5 x 10^5 cells) were plated in a 10 mm tissue culture dish and the day after 1 ml of LV was added together with 8µg/ml of hexabromide to further enhance transduction efficacy (Sigma-Aldrich, 107689). The amount of LV and the efficiency were optimized in previous experiments (protocol: https://www.addgene.org/protocols/fluorescence-titering-assay).

In these experimental settings, to reduce the probability of off-target effects, we used two different shRNA, which paired to a different sequence on STARD3 messenger RNA (Sh1: CAGGAAGAGAACTGGAAGTTT; sh2: GACCTGGTTCCTTGACTTCAA)

Functional-biochemical assays to evaluate STARD3 effects on colon cancer cell lines

To assess the extent of the effect of STARD3 and demonstrate a possible target role in colorectal cancer, we analysed the effect of STARD3 silencing evaluating the variation in terms of cell viability, colony formation capacity, anchorage-independent growth capacity, caspase 3-7 activation and apoptosis levels. All these experiments were performed in at least three different colon cancer cell lines (HCT-116, HT-29, Colo-201, Colo-205).

A) **Cell viability assay**. $1x10^3$ cells were seeded in 96-multiwell transparent microplate (Sarsted) and every 24h cell viability was measured using the CellTiter-Glo® assay system (Promega) according to the manufacturer's instructions. Luminescence was assessed with microplate reader (Infinite F1000 Pro, Tecan). The resulting values were normalized on the control pLKO empty vector, in the experiments at 96h end point, whilst in time course experiments, each cell line was normalized on its T0.

B) **Colony formation assay.** $1x10^3$ were grown in 6-well plates for 14 days to form natural colonies. Then, colonies were fixed with 4% paraformaldehyde and stained with Crystal Violet 0.05%. For colony counting/ quantification, 500µl of Methanol was added to solubilize the dye. 540nm and 630nm Absorbance values were assessed with microplate reader (Infinite F1000 Pro, Tecan).

C) **Soft agar assay.** Cells were plated in 6-multiwell plate, in duplicate, at the concentration of $2x10^4$ and $5x10^4$ per well, in 1.5 ml of Soft Agar matrix, composed by DMEM 2X (Sigma-Aldrich), Tryptose phosphate broth (T8159, Sigma), Noble Agar (BD) and FBS (Microgem), 0.35% final, over a bottom layer of Soft Agar matrix, 0.75% final. Cells

were kept in culture and medium was added weekly. Picture of the cells were taken weekly. After the 21 days, cells were fixed with 4% PFA and stained with Crystal Violet 0.05%.

D) **Caspase 3-7 activity assay.** Cells pellet were collected, proteins were extracted in NP-40 buffer (Igepal 0.5%, HEPES pH7 50 mM, NaCl 250 mM, EDTA 5 mM) then the protein content was quantified by Bradford assay. Equal amount of protein (20 µg) were added to a 96multiwell transparent microplate. Each sample was incubated with 20 µl of Caspase-Glo 3/7® kit reagents (Promega) and after 30 minutes the luminescence assessed with microplate reader (Infinite F1000 Pro, Tecan). A higher level of luminescence was indicative of higher caspase activity.

E) **Apoptosis levels.** Adherent cells were detached, washed two times with PBS (Gibco™) and collected along with floating cells and derbies at the proper timing. $1X10^5$ cells were counted, then incubated with 5µl of Annexin V-PE and 10µl of 7AAD reagents for 30 minutes at RT in the dark (PE Annexin V Apoptosis Detection Kit I - BD). Cells were acquired by flow cytometer FACS Canto (BD). The recorded events were 10000 per sample, gated using Forward Scatter Channel (FSC) and Side Scatter Channel (SSC) to select cells with the most homogeneous features, and were analyzed in term of Annexin-V and 7AAD fluorescence intensity detected by flow cytometer using FACS Diva software (BD). Early Apoptosis, Late Apoptosis and dead cells are evaluated by this method : healthy cells, Annexin V(–) and 7-AAD(–); dead cells, Annexin V(+) and 7-AAD(+); early apoptotic cells, Annexin V(+) and 7-AAD(–); late apoptotic cells, Annexin V(-) and 7-AAD(+). As mentioned in the datasheet “This assay does not distinguish between cells that have undergone apoptotic death versus those that have died as a result of a necrotic pathway because in either case, the dead cells will stain

with both PE Annexin V and 7-AAD". For this reason, Annexin V(+) and 7-AAD(+) cells are defined as "dead cells".

Establishing of mouse and human organoids

Mouse organoids were generated from tissues collected post-mortem after approval of Italian Ministry of Health, National Cancer Institute (CRO) of Aviano. Human organoids were collected with biobank informed consent at National Cancer Institute (CRO) of Aviano.

Organoids have been established from adult stem cells by mimicking the biochemical (thanks to specific growth factor) and physical signals (thanks to Matrigel) of colon tissue development and homeostasis. Briefly, mouse and human colon were collected after surgery into DMEM/F12 (Sigma-Aldrich) plus antibiotics Levofloxacin 100ug/ml-1, Vancotex 25ug/ml, Gentamicin 200ug/ml, Fungizone 5ug/ml). Biopsies were mechanically dissociated into ~1-mm pieces, then digested with 2mg/ml collagenase type I (Gibco™) in DMEM/F12 without phenol red (Sigma-Aldrich) at 37°C for 1-2h according to tissue size. After tissue digestion, DMEM/F12 media containing 10% FBS was added to the suspension to inactivate the enzymes. Optionally, tissues samples were washed in 1X RBC lysis buffer (Thermo Fisher Scientific) under gentle rotation for 10 minutes at room temperature to lyse the majority of contaminating red blood cells.

After washing in cold HBSS (Gibco™), organoids were centrifuged for 5 minutes at 1000 rpm. Then organoids pellet was suspended in 10µl of Geltrex™ LDEV-Free Reduced Growth Factor Basement Membrane Matrix (Gibco™) and seeded in pre warmed 24-well tissue culture plates. Plates were placed into a cell culture incubator at 37 °C and 5% CO2 for 20-30 min to solidify the droplets and 450uL of media was added to each well.

Mouse colon organoids were cultured in LWRN-conditioned media supplemented with 10µM of Rock inhibitor (Tocris, HY-10583), 10µM of Forskolin (MedChemExpress HY-

10071), 20ng/ml Noggin Murine(Peprotech- af-250-38) and100ng/ml R-spondin1 (Peprotech 315-32) according to Stappenbeck protocol[120]

Human colon organoids media consists of LWRN conditioned media containing Pen/Strep antibiotics (Sigma-Aldrich), Glutamax (Thermo Fisher Scientific, Waltham, MA, USA), N2 (Thermo Fisher Scientific), 50 ng/ml EGF (Peprotech), 10ng/ml Gastrina (Peprotech), 10 ng/ml FGF10 (PeproTech), 10 ng/ml FGF2basic (Peprotech) 100 ng/ml R-spondin1 (PeproTech), B27 (Thermo Fisher Scientific) and 10µM Y-27632 [115].

The culture medium was changed every 2-3 days.

Mouse colon organoids transduction

For mouse colon organoids transduction, samples were detached using Accutase sterile solution (A6964 Sigma) for 5 minutes. Accutase was inhibited with 10 ml of Dulbecco′s Modified Eagle′s Medium/Nutrient Mixture F-12 Ham (D6434, Sigma) and organoids were centrifuged for 10 minutes at 1000 rpm. After washing with HBSS (Gibco™), Cell recovery solution (Corning, 354253) was added to the pellet for Matrigel depolymerization. Then, organoids pellets were incubated for 6h in a mix containing:

-1ml Lentivirus encoding the gene of interest.

- 8µg/ml of hexabromide (Sigma-Aldrich, 107689).

-10µM of Rock inhibitor (Tocris, HY-10583).

1 ml of organoid culture medium was added to the organoid-virus mixture and transferred into an eppendorf tube and centrifuge in a microcentrifuge for 5 min at 1000 rpm to pellet organoids. Supernatant was removed and the pellet resuspended in ice-cold Matrigel.

10µl droplets were seeded in the middle of a well in a 24 wells plate and incubate in culture incubator at 37 °C for 20-25 min to solidify, Lastly, carefully 400μl of mouse colon organoid culture medium (homemade LWRN-conditioned media) supplemented with Primocin (ant-pm-

05 Invivoge), 10μM of Rock inhibitor (Tocris, HY-10583), 10μM of Forskolin (MedChemExpress HY-10071), 20ng/ml Noggin Murine (Peprotech- af-250-38) and 100ng/ml R-spondin1 (Peprotech 315-32) were added.

After 3 days medium was refreshed and supplement with a selection antibiotic. We use this commercially available plasmid:

-pLV-beta-catenin deltaN90 (human) (Addgene 36985). This plasmid confers resistance to G-418 antibiotic.

- pLenti-PGK-KRAS4B(G12V) (human) (Addgene 35633). This plasmid confers resistance to Hygromicin

As it concerns STARD3, we use the plasmid PLX304 in which we insert the entire sequence of the human gene plus a tag called V5 TAG. The sequence of the tag is GGT AAG CCT ATC CCT AAC CCT CTC CTC GGT CTC GAT TCT ACG. This plasmid confers resistance to Blasticidin.

To obtain organoids with the double mutation (β-Catenin and STARD3 over-expression), they were first infected with pLV-beta-catenin deltaN90 and then, after antibiotic selection, with PLX304. pLenti-PGK-KRAS4B(G12V) was used as a positive control for the second infection.

Functional-biochemical assays to evaluate STARD3 effects on mouse colon organoids

To assess the extent of the effect of STARD3 and demonstrate a possible oncogene role in colorectal cancer, we analysed the effect of STARD3 over expression (CMV promoter) evaluating the variation in terms of cell growth, size increasing, anchorage-independent growth capacity. All these experiments were performed in triplicate.

A) **Organoids growth rate assay**. Organoids were seeded in 96-multiwell transparent microplate (Sarsted) in 2μl Matrigel drop (Corning). Every 24h, cells proliferation was measured via the measurement of ATP levels using the CellTiter-Glo 3D

reagent (Promega), according to the manufacturer's protocol. Luminescence was assessed with microplate reader (Infinite F1000 Pro, Tecan). The resulting values were normalized on the control V5-luciferae vector, in the experiments at 96h end point, whilst in time course experiments, each cell line was normalized on its T0.

B) **Size analysis.** Organoids were seeded in 96-multiwell transparent microplate (Sarsted) in 2μl Matrigel drop (Corning) Images were taken on Nikon eclipse ts2r inverted microscope using a 2X objective The size ratio between each experimental condition and control group was calculated by comparing the mean value for the experimental condition group with the mean value of the control group. The size of each organoid (V) was quantified using ImageJ.[121]

Immunohistochemistry

Mouse colon organoids and patient derived organoids were collected using cell recovery solution (Corning) to remove Matrigel and processed as previously described.[122]

Briefly, Organoids were fixed in 4% PFA solution for 20 minutes and, after two times cold HBSS washing, they were embedded in 1% agarose. Organoids in agarose solution were paraffin-embedded following dehydration in alcohol and clarification in xylene. From paraffin blocks, 2µm multiple serial sections on a microtome were cut.

To remove paraffin wax, sections were placed in fresh xylene containing jars for two times for 5 minutes each. Then for the rehydration, sections were placed in decreasing scale of 100%-90%-80%-50% ethanol solution. To complete the rehydration process, sections were washed two-times in dH2O for 5 minutes each. Sodium Citrate (10mM pH 6 for 20 minutes at 98°C and 20 minutes at room temperature) antigen retrieval solution was used. Following steps including washing, hydrogen peroxide block and non-specific signal block, secondary antibody

and staining were performed using Epredia™ UltraVision LP HRP Polymer & DAB Detection System according manufacture instructions.

Primary antibody was incubated overnight at 4°C in TBS-BSA 0,05%. Primary antibodies are reported in the table.

Table 2 Primary antibody for IHC analysis

Antibody	Producer	Cat. number
MUC2	Abcam	ab272692
CK-20	Abcam	ab97511
CK-7	Abcam	ab181598
CDX-2	Abcam	ab76541
STARD3	Abcam	Ab3478

Lastly, sections were counterstained (5 second in Harris hematoxylin), washed whit water in the sink and dehydrate with an increasing ethanol scale 50%-80%-90%-100% and xylene for 5 minutes.

Western blot

Cells were collected using a scraper, washed two times with PBS (Gibco™) to remove traces of medium, centrifuged and kept on ice. Organoids were collected using Cell Recovery Solution (Corning) for 1h on ice, washed two times with HBSS (Gibco™) and centrifuged to get the pellet.

Sample pellets were then lysed using RIPA buffer (50 mM Tris-HCl pH 8.0, 150 mM NaCl, 1% IGEPAL, 0.5% sodium deoxycholate and 0.1% SDS) supplemented with sodium orthovanadate (Sigma-Aldrich, S6508) and sodium fluoride (Sigma-Aldrich, S6776) Protease Inhibitor Cocktail (Roche, 04693116001) or phosphorylated proteins lysis buffer (10mM Tris-HCl, 2mM EDTA, 1% SDS) supplemented with Protease Inhibitor Cocktail (Roche,

04693116001), sodium orthovanadate (Sigma-Aldrich, S6508) and sodium fluoride (Sigma-Aldrich, S6776) according to the final target. Protein concentration was estimated by Bradford assay by using Bio-Rad Protein Assay Dye (Bio-Rad, according to manufacture instruction. Samples were prepared using equal amounts of protein (25-30μg), 5X Sample Buffer (GenScript, MB01015) and diluted to a final volume of 25μl with RIPA buffer. Samples were heated at 95°C for 10 minutes and proteins were separated by 4-20% SDS-polyacrylamide gel electrophoresis (GenScript, M42012) and transferred to nitrocellulose membrane (GE Healthcare, 10600002) using Mini-PROTEAN Tetra Vertical Electrophoresis Cell (Bio-Rad, 1658004). The protein signal was detected with LiteAblot® EXTEND Chemiluminescent Substrate (Euroclone, EMP013001) using VWR® Imager CHEMI Premium (VWR, 730-1469P) and images were analyzed using ImageJ software (Schneider et al., 2012).

The secondary antibodies used are Goat anti-Mouse IgG (Invitrogen, 31430), Goat anti-Rabbit IgG (Invitrogen, 32460), and Rabbit anti-Goat IgG (Invitrogen, 31402). Primary antibodies are reported in the table 3.

Table 3 Primary antibody for Western blot analysis

Antibody	Producer	Cat. number
STARD3	Santa Cruz	sc-390040
β-Catenin	Cell Signaling	8480S
KRAS (G12V Mutant Specific)	Cell Signaling	14412
c-Myc (-tag)	Bethyl	A190-104A
V5 Epitope Tag	Millipore	3286106
HA-TAG	Roche	11583816001

Patient derived colon cancer organoids drug screening

Cancer organoids were obtained from anonymized specimens. Biobank informed consent for research purposes was available to collect the samples at the National Cancer Institute (CRO) of Aviano, Italy.

Patient information including clinical characteristics, treatment age, sex, race, tumour location and histotype, year of diagnosis, primary tumour size, histological grade, number of positive lymph nodes, vascular invasion, stroma to tumor ratio, budding, application of adjuvant therapy, and follow-up.

After the establishment of cancer-derived organoids, organoids were dissociated using accutase and re-seeded in Matrigel into a 96-well plate in four replicates. Organoids were cultured in complete media until small organoids were formed then were treated with serial dilution of first-line chemotherapy agent (5-FU, oxaliplatin and irinotecan), regorafenib and STARD3 inhibitors. After 96h treatment. Viability was measured via the measurement of ATP levels using the CellTiter-Glo 3D reagent (Promega), according to the manufacturer's protocol. Luminescence was detected using Infinitie 1000 Tecan reader. Drugs efficacy were evaluated using IC_{50} value (defined by FDA as the minimal concentration of a drug that is required for 50% inhibition *in vitro*) and results were plotted using GraphPad Prism.

Fluorescence in situ hybridization (FISH)

Fluorescence In Situ Hybridization was used to detect STARD3 amplification, specifically Copy Number Variation, in a selected group of colorectal cancer patients. As there is no probe available on the market, we have designed our custom dual FISH probes: one STARD3 locus-specific 5-TAMRA fluorophore-labeled probe (orange) and one centromere Chromosome 17 5-fluorescein-labaled probe (green).

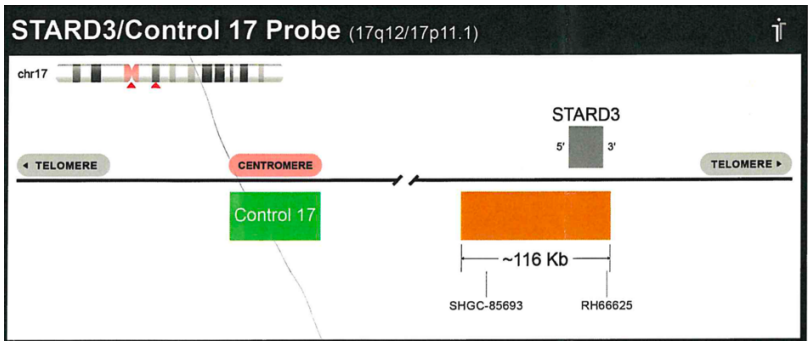

Figure 11. Custom FISH probe for STARD3 detection in colorectal patients' tissues.

FISH was be performed with our internal validated protocol. Technically, 5µm slices were heated in the stove at 56°C for 2h. Slices were rehydrated with xylene for 3 times each lasting 10 minutes, then ethanol 100% for 2 times each lasting 5 minutes, ethanol 96% for 2 times each lasting 5 minutes, ethanol 75% for 2 times each lasting 5 minutes. Antigen retrieval was performed at 98°C in TE buffer 1x solution (obtained by diluting a TE solution 10x made of 5 parts of Tris HCl 5mM and 1 part of EDTA 1 mM) for 15 minutes. After washing with milliQ Water, digestion was performed in Pepsin-HCl solution at 37°C for 4 minutes in the TermoBrite® (37°C). Then, a drop (2-3 μL) of reconstituted probes solution was added and covered with a 1x1 cm coverslip. Lastly slices were incubated in the TermoBrite® at 37°C Overnight. The day after, saline-sodium citrate (SSC) buffer was used to increase the stringency of the hybridization. Lastly, nuclei were counterstained with VECTASHIELD® Antifade Mounting Medium with DAPI (Vector laboratories, H-1200-10). Pictures were taken with LEICA DM5500 B fluorescent microscope and at least 200 cells were analyzed using CytoVision imaging software.

Mice and animal studies

Animal experiments (EU directive (2010/63/EU) were performed under the authorization of the National Ethical Committee and the Administration of the Republic of

Slovenia for Food Safety, Veterinary and Plant Protection and Italian Ministry of Health (CRO, Aviano). 4-weeks old Immuno-deficient nude mice were purchased from Emvigo. Ear clipping was used for animal recognition. Animals were caged together and treated in the same way. We performed two different studies:

-HCT-116 Wild-Type versus HCT-116 with STARD3 knock-down

-Mouse colon organoids Wild-Type VS mouse colon organoid with β-Catenin and STARD3 over-expression (selected with 2ug/ml of Blasticidin and 100ug/ml of G-418 sulphate).

After the lentiviral transduction, cell lines and mouse colon organoids were propagated for two weeks. Organoids were detached mechanically, washed two times with HBSS (Gibco™) and resuspended in 30% Corning® Matrigel® Matrix High Concentration (HC), Phenol-Red Free, LDEV-free diluted in Dulbecco′s Modified Eagle′s Medium/Nutrient Mixture F-12 Ham without phenol red and without FBS (D6434, Sigma). An aliquot was completely dissociated with Accutase for cell counting. Organoids corresponding to $1x10^6$ cells were injected into both side of the dorsal skin of nude mice.

Cell lines were detached with Trypsin 0,05% (Sigma-Aldrich), washed with PBS (Gibco™) and resuspended Geltrex™ 50% LDEV-Free, hESC-Qualified, Reduced Growth Factor Basement Membrane Matrix in PBS (Gibco™). $5x10^6$ cells were injected into both sides subcutaneously.

Tumour growth was monitored using calipers weekly, and animals were euthanized when tumour volume is >1500 mm^3 (humane endpoint). Volumes were calculated using the formula: volume = $(l^2 \times L)/2$, where L is the long side and l is the short side of each tumour. Tumours were harvested, weighed, fixed in formalin and paraffin embedded for pathological analysis.

Statistical analysis

All the experiments were performed in triplicate and the p-value was calculated using a two-tailed Student's t-test using GraphPad Prism. P values are expressed as follows:

* $P \leq 0.05$, ** $P \leq 0.01$, *** $P \leq 0.001$ and **** $P \leq 0.0001$.

Results

STARD3 is overexpressed in colorectal cancer tissue

It has been previously reported /www.proteinatlas.org/ENSG00000131748-STARD3/pathology/colorectal Revision 15 December 2022) in Protein Atlas Database that STARD3 is expressed in colon cancer tissue. In their cohort, 62,98% of tumour samples show high STARD3 levels (376 out of 597) and it is correlated to a low 5-years survival. In our laboratory at I.R.C.C.S Centro di Riferimento Oncologico di Aviano STARD3 protein level was analyzed on tissue microarray of 46 cases of colorectal cancer patients and the corresponding healthy tissue by IHC. The IHC staining was converted to an H-score. The H-score from 0 to 75 (median value) was defined as low expression and > 75 was defined as medium-high expression. In our patient cohort, 4 out of 46 healthy tissues and 23 out of 46 tumour tissues showed high levels of STARD3 (Fig.12).

Tissue microarray summary	Low	High	TOT
CRC	21	23	44
Normal	40	4	44
P-value			**<0.0001**

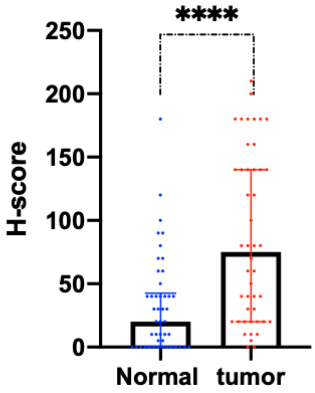

Figure 12 IHC analyses on tissue microarray of 44 cases of colorectal cancer patients and adjacent tissues. *The IHC staining was converted to an H score: intensity (0, 1, 2, 3) x area (0-100%). The H score from 0 to 75 (median) was defined as low expression and > 75 was defined as medium-high expression. Plot with median and interquartile range.*

The analysis also showed that in only two patients the healthy tissue has a higher H-score than the tumour tissues (n15 and n22), in three patients the H-scores is equal (n12, n18, n24), while in the remaining 39 patients the tumour tissue have higher H-scores than normal colon (Table 4).

patient Number	Normal			Tumour		
	Positivity	Intensity	H-score	Positivity	Intensity	H-score
1	30	1	**30**	90	2	**180**
2	0		**0**	90	2	**180**
3	10	1	**10**	80	2	**160**
4	90	1	**90**	90	2	**180**
5	40	1	**40**	70	2	**140**
6	60	1	**60**	80	1	**80**
7	40	1	**40**	100	2	**200**
8	60	1	**60**	70	2	**140**
9	70	1	**70**	90	2	**180**
10	40	1	**40**	90	2	**180**
11	70	1	**70**	90	2	**180**
12	50	2	**100**	50	2	**100**
13	50	1	**50**	60	2	**120**
14	30	1	**30**	70	2	**140**
15	30	1	**30**	10	1	**10**
16	10	1	**10**	30	1	**30**
17	10	1	**10**	60	1	**60**
18	40	1	**40**	20	2	**40**
19	10	1	**10**	20	2	**40**
20	20	2	**40**	50	1	**50**
21	20	1	**20**	20	2	**40**
22	40	1	**40**	30	1	**30**
23	30	1	**30**	60	2	**120**
24	10	1	**10**	10	1	**10**
25	5	1	**5**	70	1	**70**
26	0		**0**	10	2	**20**
27	0		**0**	10	2	**20**
28	0		**0**	20	1	**20**
29	0		**0**	30	2	**60**
30	20	1	**20**	40	2	**80**
31	0		**0**	5	1	**5**
32	60	3	**180**	70	3	**210**
33	0		**0**	10	2	**20**
34	0		**0**	10	2	**20**
35	20	1	**20**	70	2	**140**
36	0		**0**	80	2	**160**
37	0		**0**	20	1	**20**
38	60	2	**120**	70	2	**140**
39				70	2	**140**
40	40	1	**40**	40	2	**80**
41	0		**0**	40	2	**80**
42	0		**0**	20	1	**20**
43	5	1	**5**	10	1	**10**
44	0		**0**	20	2	**40**

Table 4 tissue microarray summary table. STARD3 expression levels (quantified by H-SCORE) in healthy tissue and tumour tissue from 44 patients are compared.

STARD3 knock-down inhibits colon cancer cell growth *in vitro*

Because STARD3 expression is elevated in colorectal cancer tissues, we investigated the effect of STARD3 suppression on colon cancer cell lines. Several *in vitro* experiments were performed. First, STARD3 expression was stably knocked down in the human colon cancer cell lines HT-29, HCT-116, COLO-205 (Fig.13). Optimal conditions, including number of cells, lentivirus titration and time point were established in previous set up experiment (data no show) In these experimental settings, to reduce the probability of off-target effects we used a second shRNA (sh2) in addition to the previous, which paired to a different sequence on STARD3 messenger RNA.

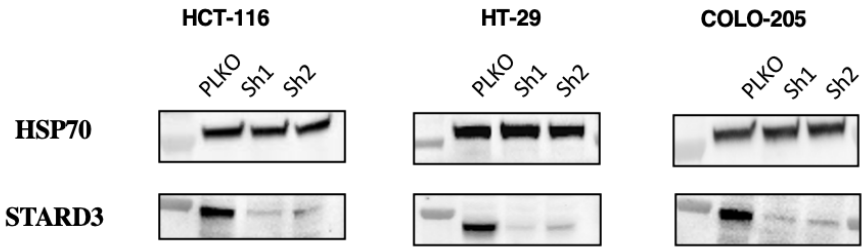

Figure 13 STARD3 Knockdown*. was evaluated by western blot analysis The difference between PLKO and KD cells was statistically significant.*

Then we analyzed the effect of STARD3 silencing evaluating the variation in terms of cell viability, colony formation capacity, and anchorage-independent growth capacity. The effect of knockdown on the viability was monitored every 24 hours, for 96 hours, and we observed a severe and robust reduction of vitality in all the cells knockdown for STARD3.

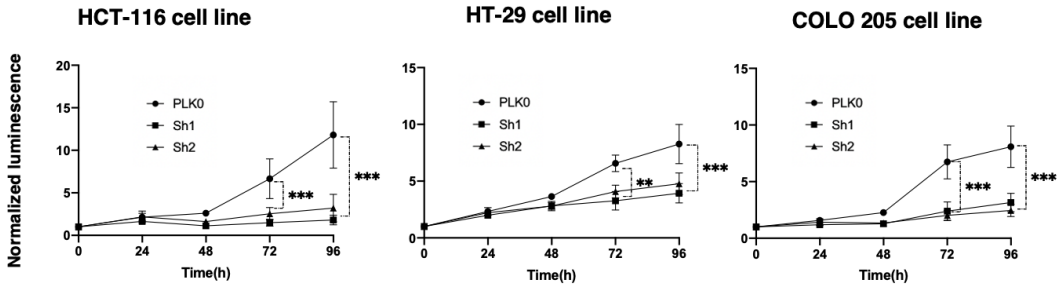

Figure 14. **Growth curve** *STARD3 was KD with 2 shRNA in 3 different cell lines and viability was measured with a MTT-like assay. Y axis represents the ratio between KD/PLK0 shRNAs (luminescence). X axis represents the time (hours)*

Clonogenic assay or colony formation assay is an *in vitro* cell survival assay based on the ability of a single cell to grow into a colony. In our experiments, the colony formation rate of STARD3 knock down cells was dramatically suppressed compared to the control (Fig.15).

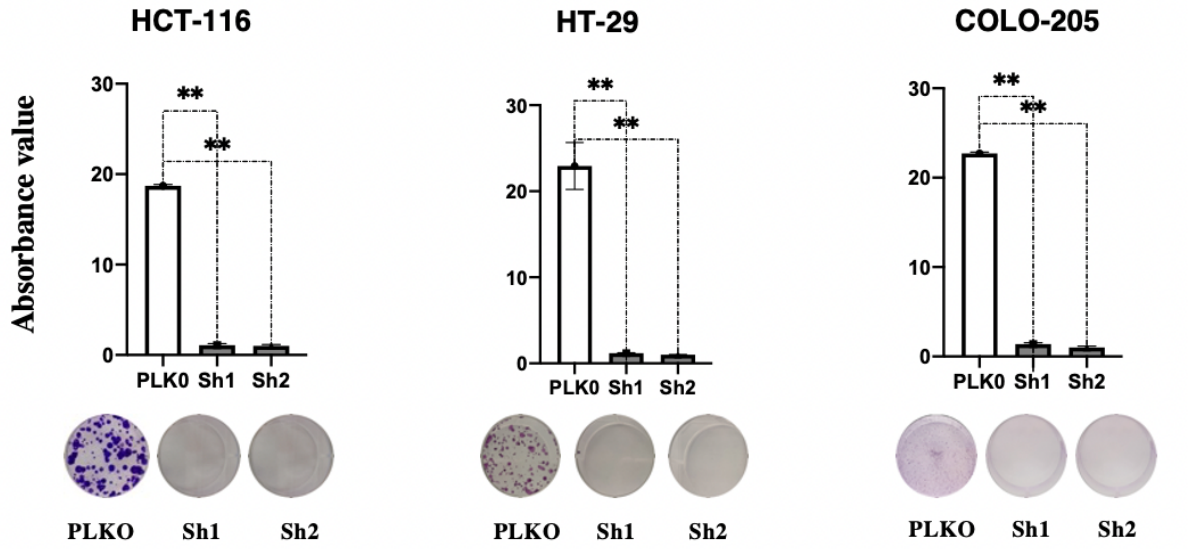

Figure 15. Colony formation assay*. STARD3 was KD with 2 shRNA in HCT-116, Colo-205 and HT29 cell lines. The cells were plated as single cells and the colonies were stained with crystal violet solution after 21 days. The difference between PLKO and KD cells was statistically significant, p-value < 0.01*

Anchorage-independent growth is a key feature of oncogenic transformation and can be measured by soft agar assay. The ability of sustaining cell growth independently from external mechanical stimuli, such as interaction with a solid substrate, is another hallmark of cancer. [123] To evaluate the role of STARD-3 on anchorage-independent growth, shSTARD3-transduced cells were seeded into a soft matrix and cultured for 21 days. Pictures were taken during the culture and afterwards cells were stained with crystal violet. The results have shown that when STARD3 is silenced, spheroids are smaller, or they are not able to growth in soft agar (Fig.16)

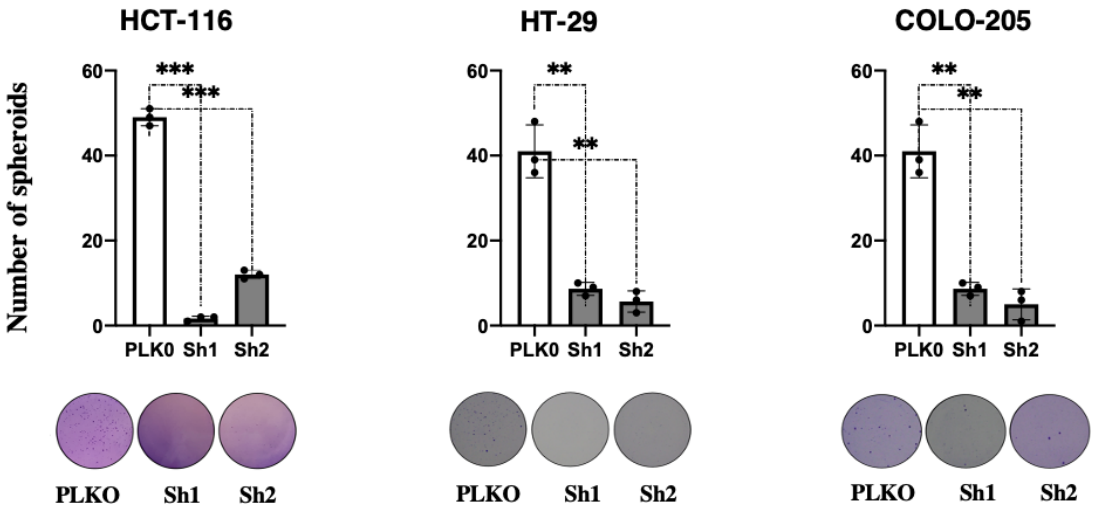

Figure 16. Soft agar assay*. HCT-116, HT-29 and COLO-205 cell line was plated on soft agar and the colonies were stained with crystal violet solution after 21 days. The images represent two independent experiments. The difference between PLKO and KD cells was statistically significant, p-value < 0.01.*

STARD3 Inhibition induces apoptosis in Colorectal cancer cell lines

We then investigated whether STARD3 inhibition could result in apoptotic activation. We evaluated the expression of the apoptotic marker Annexin V by flow cytometry. Interestingly, the analysis revealed that, after STARD3 knock-down, cells started to express more apoptotic markers compared to the control and, despite differences among the cell lines, both single positive (Annexin V alone) and double positive (Annexin V and 7AAD) populations were from at least twice more concentrated than the control.

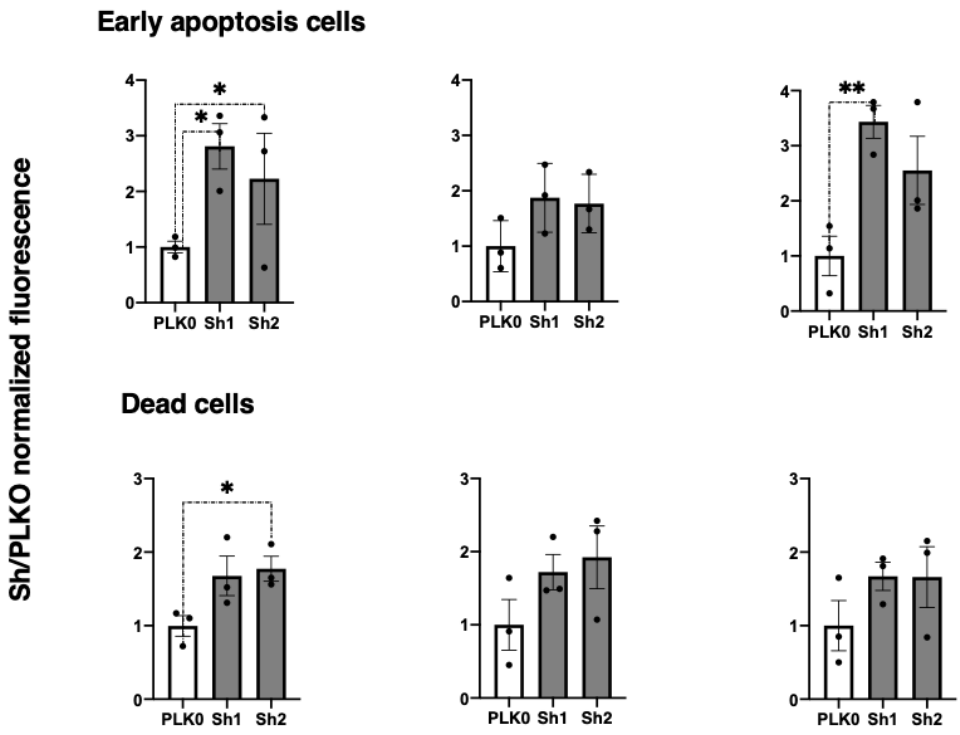

Figure 17 Relative amount of Annexin-V positive HCT116, COLO-205, HT29 silenced and control cells*. Cell lines were collected 72h days after transduction Cells were acquired by flow cytometer FACS Canto (BD). The recorded events were 10000 per sample, gated using Forward Scatter Channel (FSC) and Side Scatter Channel (SSC) to select cells with the most homogeneous features, and were analyzed in term of Annexin-V and 7AAD fluorescence intensity detected by flow cytometer using FACS Diva software (BD).*

The pro-apoptotic phenotype resulting from STARD3 inhibition was further supported by the detection of the activation of caspase-3 and -7, the main and final effectors of apoptotic pathway. Using a luminescence assay that detected caspase activity, apoptosis levels were

analyzed in HCT-116, COLO-205 and HT-29. The results show a significant increase of caspase activity compared to the control.

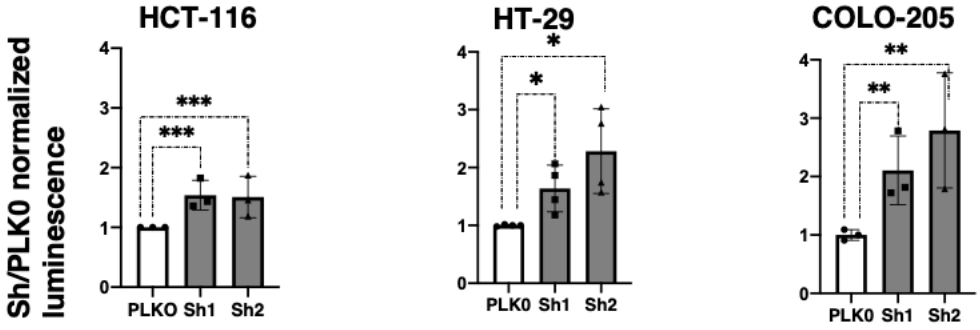

Figure 18 STARD3 silencing induces caspase activation in HCT-116, HT-29, Colo-205*. activity of caspase 3/7 proteins was assessed with Caspase-Glo® 3/7 Assay (Promega). Y axis, normalized luminescence KD/PLK0*

STARD3 knock-down inhibits tumour growth *in vivo.*

To understand if STARD3 is a valid therapeutic target in colorectal cancer, we established a murine xenograft model to verify the role of STARD3 *in vivo*. HCT-116 wild type and STARD3 Knock-down cell line were injected in four thymic nude mice ($3*10^6$ cells in 30% high concentrated Matrigel). After 50 days, in all HCT-116 wild type mice tumor with volume >1000 mm^3 were measured while in HCT-116 STARD3 knock-down mice no tumor mass was observed. Log-rank (Mantel-Cox) statistical test confirmed that difference is significant (P value < 0.05)

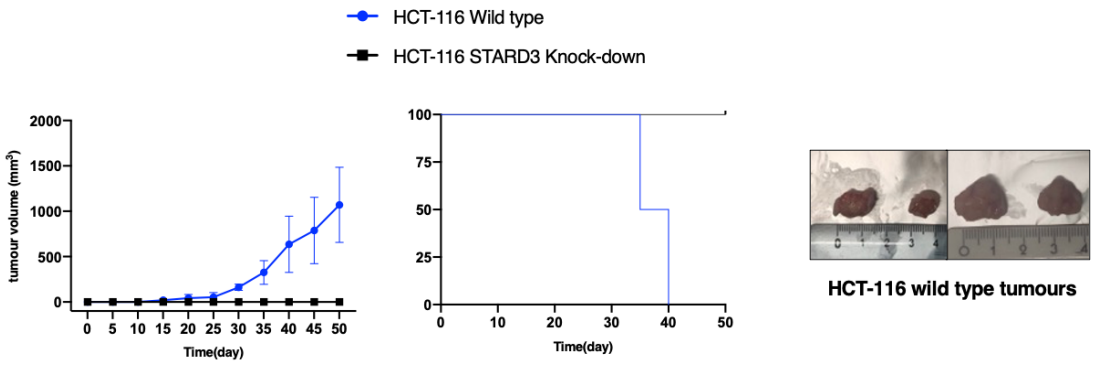

Figure 19. STARD3 suppression inhibits colon cancer cell growth in vivo*. Left: mice tumour measurement. Right: Kaplan-Meier tumor-free mouse survival curves. The survival of mice from the date of injection until the detection of palpable non regressing tumors (>400 mm^3). Number of mice=4*

STARD3 promotes the growth and size increasing of mouse colon organoids.

To dissect the role of STARD3 in colorectal cancer in a more physiological environment, we overexpress STARD3 in mouse colon organoids by lentiviral infection. After antibiotic selection, our results show that STARD3 overexpression enhances colony-forming potential of small intestinal organoids with a simultaneous increase in the size and growth rate of organoids compared to the control and with results comparable to the overexpression of β-catenin. On the other hand, the simultaneous over expression of genes (β-catenin+STARD3 OE) did not lead to any further increase in growth and size of the organoids.

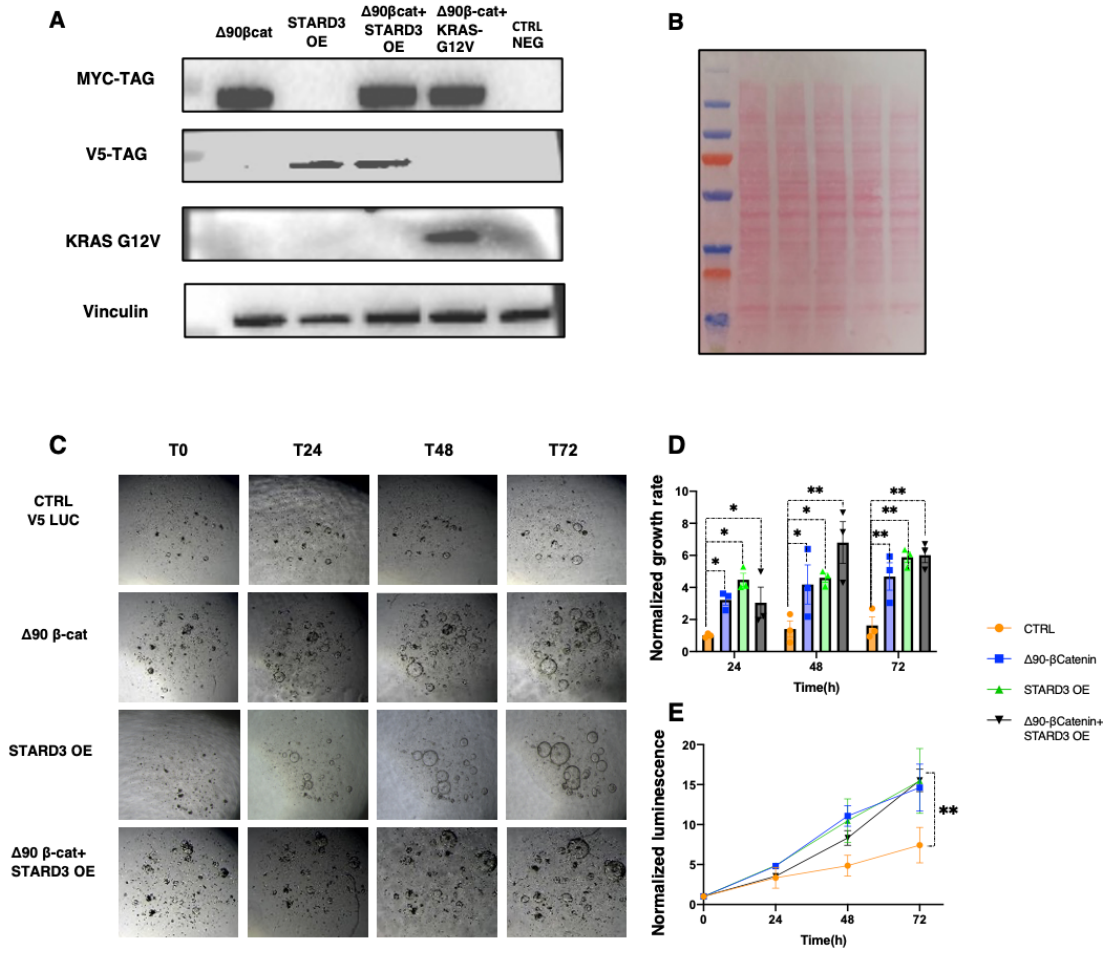

Figure 20. *Up: western blot analysis to confirm the overexpression of our proteins of interest by plasmid tags. KRAS G12V was used as a positive control for the second infection (A-B). Down: mouse colon organoids size analysis and growth curve: comparison between CTRL and STARD3 overexpressed organoids. Illustrative image of infected organoids in culture followed over time (C).Overexpression of STARD3 significantly enhanced the organoids size compared with the control (D) Overexpression of STARD3 significantly enhanced organoids proliferation compared with the control (E)*

STARD3 induces tumours formation *in vivo* when overexpressed with β-catenin

To further confirm the role of STARD3 *in vivo* we generated organoids carrying various combinations of driver gene mutations. We subcutaneously injected both side into immunodeficient mice: control V5-luc organoids, β-catenin OE organoids, STARD3 OE organoids and β-catenin+STARD3 OE organoids. In our experiment, the results showed that STARD3 induces tumour formation when over-expressed with β-catenin in 3 out of 4 mice (6 tumors in total). Log-rank (Mantel-Cox) statistical test confirmed that difference is significant (P value < 0.05)

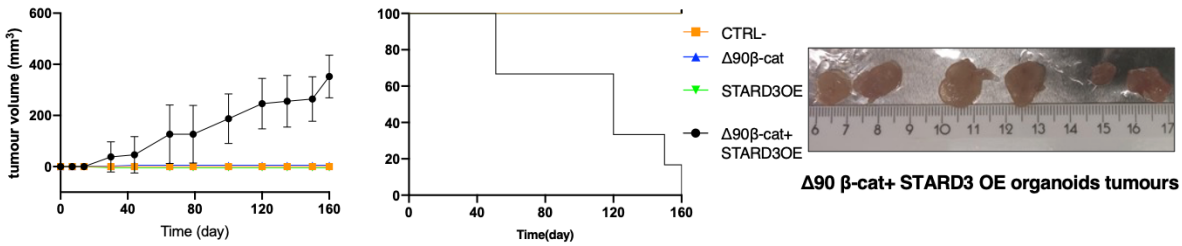

Figure 21 STARD3 induces tunour formation in vivo. *Left: mice tumour measurement. middle: Kaplan-Meier tumor-free mouse survival curves. The survival of mice from the date of injection until the detection of palpable non regressing tumors. Right: tumour picture. Number of mice =4 each group.*

STARD3 Inhibitor VS1 is effective on a subset of colorectal Patient-derived organoids, and it is linked to STARD3 expression level.

We then tested STARD3 inhibitor activity on patient-derived human organoids. Organoids can be grown from patient-derived tumour tissues, potentially enabling patient-specific drug testing and the development of individualized treatment regimens. In our preliminary study, we generated colorectal cancer organoids from 20 patients. They recapitulate histological and genetic features of original tumours including STARD3 expression level (Fig.22). The following markers were chosen as they are used in diagnostics for the differential diagnosis of colon cancer (https://www.pathologyoutlines.com/colon.html).

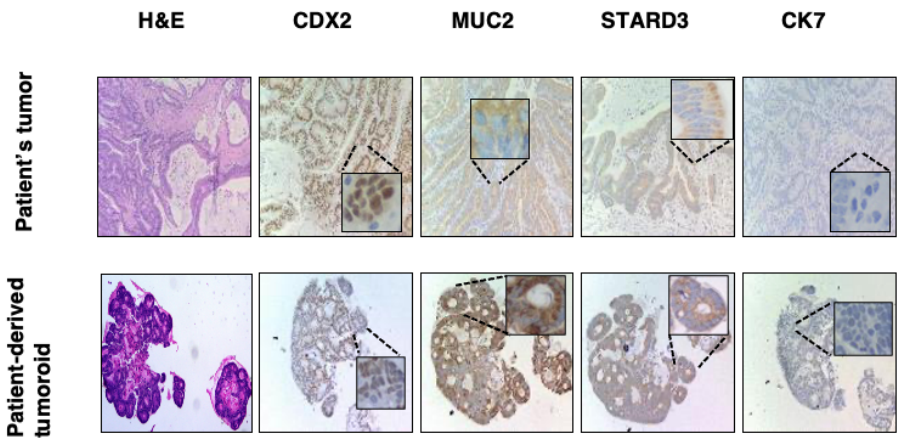

Figure 22 Example of comparison of colorectal cancer marker parent tumor versus patient-derived tumoroids*. Magnification 20X. CDX2 is a transcription factor expressed specifically in the intestine and it is involved in the maintenance of intestinal cell types. MUC2 is part of the mucin family and characteristically observed in goblet cells of small and large bowel mucosa. CK7 is cytokeratin expressed in the gut epithelia. Different CK7 expression patterns are commonly used to distinguish colorectal adenocarcinomas. Most colorectal cancers are CK7 negative (and CK20 positive (not show)). Description adapted from https://www.abcam.com/cancer/colorectal-cancer-biomarkers*

Then cancer organoids were treated with a serial dilution of first-line chemotherapy agents (5-FU, oxaliplatin and irinotecan), regorafenib and VS1.

It was possible to identify two groups of patients: one group of patients, defined as VS1 sensitive, in which the IC_{50} of STARD3 inhibitor is comparable or even lower than the first-line drugs, while the second group, defined as VS1 resistant in which the IC_{50} values are at least double that of first-line drugs (usually values above100µM).

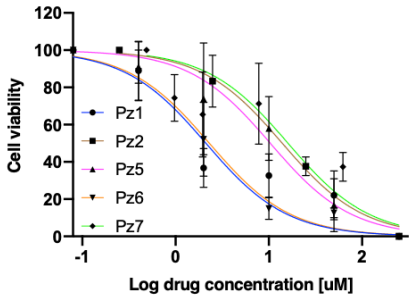

IC_{50}(µM)	VS1	5-Fluoracil	Oxaliplatin	Irinotecan	Regorafenib
Patient1	2.1±0.5	26.4±4.9	10.1±6.2	7.69±2.1	16.7±4.4
Patient2	8.9±6.0	7.6±2.8	14.6±4.8	3.2± 2.4	35.1±28.6
Patient5	7.7±4.4	34.1±4.1	14.6±11.9	>200	17.9±5.7
Patient6	1.7±1.2	13.6±3.7	21.9±6.2	>200	13.4±4.9
Patient7	16.8±8.2	31.5±3.4	17.9±5.8	82.7±21.7	17.1±4.9

Figure 23 IC_{50} on patient derived organoids with STARD3 inhibitor VS1*. The activity was evaluated in serial dilution starting from 200µM. Organoids viability was measured with a MTT-like assay (Cell titer 3D Promega). VS1 sensitive organoids show IC_{50} between 2-20 µM, while the second group, defined as VS1 resistant, IC_{50} values are higher than 100µM (not reported).*

We then used the FISH technique to assess whether patients had alterations in STARD3 levels. The results showed that 4 out of 5 VS1-sensitive patients had copy number alterations

(3 or more copies of the gene in at least 20% of cells) of STARD3 while 15 out of 15 VS1 treatment-resistant patients had no alterations (2 copies of the gene). Cut-off and number of cells were were based on our internal validated protocol for IVD (*in vitro* diagnostic) FISH probes.

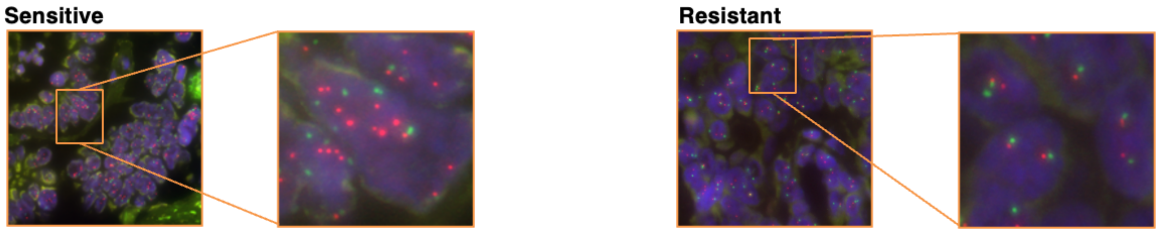

Figure 24 FISH on Colorectal Cancer. Cut-off of 20% (40 out of 200 cells) of positive cell was used to discriminate positive and negative tissues.

Discussion and Conclusion

Colorectal cancer (CRC) represents one of the leading causes of cancer worldwide, with a prevalence of more than a million cases every year. Relatively 25% of patients present metastases at initial diagnosis and approximately 50% will develop metastases, concurring to the high mortality with overall five years survival rate less than 10% for stage IV.[1]

The backbone of first-line treatment in CRC involves traditional systemic chemotherapy drugs (5-FU, oxaliplatin and irinotecan) associated with molecularly targeted treatments based on RAS mutations (Bevacizumab for RAS mutant CRC, Cetuximab or Panitumumab for RAS wild-type CRC) and microsatellite status (pembrolizumab or nivolumab for MSI-H or deficient DNA mismatch repair CRC)

Although many improvements in cancer treatment have been made, only a fraction of the tumours responds to available therapies, including combinatorial therapies, requiring a better molecular understanding of the disease in precision oncology. Nevertheless, chemotherapy is associated with certain limitations, such as existing systemic toxicity, unsatisfying response rate, unpredictable innate and acquired resistance. The estimated deaths in 2021 from colorectal cancer was approximately 900.000 worldwide. There is a crucial need for new diagnostic and therapeutic biomarkers to reduce CRC-related deaths.[3] The research is continuously searching new perspectives in order to provide the best possible outcome for all patients. In this scenario, cholesterol metabolism has received increasing attention due to its role in cancer development. Cancer cells show higher levels of intracellular cholesterol compared to normal cells. Tumor cells require high amounts of lipids, nucleic acids and proteins for their survival. Cancer cells increase the *de novo* lipid biosynthesis including cholesterol synthesis. Cellular cholesterol metabolism, including intracellular distribution, is highly coordinated and controlled by a complex protein network. Between them, StAR-related lipid transfer domain-3 (STARD3) regulates the shuttling of cholesterol across different membranes

of the cellular compartments. Whereas its specific mechanism of action in tumour cells is still under investigation, several studies have revealed its role in cancer, and it is linked to worse overall survival (OS), relapse-free survival (RFS) and disease metastasis-free survival (DMFS). Moreover, our research group has already published research article in which the first STARD3 inhibitor was validated.[82] On these bases,STARD3 has been identified in our group as a potential new therapeutic target in colon cancer.

It has been previously reported in protein atlas database that STARD3 is overexpressed in colorectal cancer tissues. To validate this, immunohistochemistry analysis was performed in a series of colorectal normal tissues (n = 44) and CRC tissues (n = 44). We found that STARD3 level was significantly higher in CRC tissues than in adjacent normal tissues (Fig. 12).

In our patient cohort, an arbitrary value of 75 (obtained from median analysis) has been chosen to discriminate samples as low STARD3 or high STARD3 expressions. The results showed that 4 healthy tissues had high STARD3 levels (H-SCORE >75). However, the corresponding tumour tissues from the same patients showed even higher levels. On the other hand, 21 tumour tissues have low levels of STARD3. The corresponding healthy tissues from the same patients showed even lower levels of STARD3. In summary, in 39 patients, tumour tissue had higher levels of STARD3 expression than healthy tissue. STARD3 expression was increased in all stages of CRC compared with that in normal tissue. Hence, these data indicate that STARD3 is overexpressed in all stages of CRC at protein level.

Because STARD3 expression is elevated in CRC, we investigated the effect of STARD3 suppression in cell survival and growth. STARD3 expression was stably knocked down in the human colon cancer cell lines HCT-116, HT-29 and COLO-205, detecting a considerable decrease of the protein's level (Fig. 13). The effect of knockdown on the viability was monitored every 24 hours, for 96 hours and we observed a substantial and robust reduction of vitality in all the cells knockdown for STARD3. To support these data, we performed colony

formation assay and soft agar assay. Colony assay essentially tests every cell in the population for its ability to enable replicative immortality, one of the hallmarks of cancer. Soft agar assay measures anchorage-independent growth capacity and it is another hallmark of cancer. By the analysis, it was evident that STARD3 inhibition had a drastic effect on these two hallmarks: cancer cells are not able to form colony and they are not able to growth (Fig.15 and Fig.16). Collectively, these results suggest that STARD3 is essential for colon cancer cell survival and growth *in vitro.*

Given the drastic effect of STARD3 silencing on tumour cell growth capacity, we investigated whether this process could result in apoptotic activation. We evaluated the expression of the apoptotic marker Annexin V. Interestingly, the analysis revealed that, after STARD3 knock-down, cells started to express more apoptotic markers compared to the control. The increase in the apoptotic population was detected in all the cell lines analyzed, however only in HCT-116 the difference between the silenced and control cells was statistically significant. In HT-29 and COLO-205 a trend toward an apoptotic increase was seen, despite the wide variation of the standard deviation. For this reason, to support these findings we analyzed the caspase-3 and -7. Caspases levels were analyzed upon STARD3 silencing, showing a significant increase of caspase activity compared to the control.

Despite the variability amongst different cell lines, we showed a clear involvement of STARD3 in the apoptotic process, which suggest that STARD3 may play a role as anti-apoptotic protein, another hallmark of cancer. Finally, we established a murine xenograft model to verify the role of STARD3 *in vivo*. In HCT-116 STARD3 knock-down no tumour mass was observed (Fig.19)

Literature data show high cholesterol levels inhibited cell apoptosis in colorectal cancer cell lines. [124]. In addition, increased cholesterol levels in mitochondria are anti-apoptotic and support the ability of mitochondria to generate energy and synthesize steroid hormones to foster

growth and progression in several cancers[52]. Therefore, we can speculate that targeting STARD3 blocks cholesterol transport by inhibiting cell growth inducing apoptosis, thus supporting the target potential of this protein.

To dissect the role of STARD3 in colorectal cancer in a more physiological environment, we overexpress STARD3 in mouse colon organoids by lentiviral infection. STARD3 overexpression enhances the growth and the size of organoids derived from normal colon crypts (Fig.20). It is possible to postulate that it is due to the increased availability of cholesterol and its increase at the plasma membrane level, as demonstrated by Vasillev and colleagues in breast cancer cells.[83]

Furthermore, the results are comparable with those in organoids with pLV-beta-catenin deltaN90 (human). This model simulates the first hit of the adenoma-carcinoma sequence of colon cancer in that there is a constitutive activation of the protein (as occurs with APC deletion). We therefore generated organoids with the double mutation but did not notice an increase in size and growth compared to the single mutations. However, the injection of these organoids led to the formation of tumours (6 out of 6) in nude mouse models, whereas no tumour masses have grown in mouse models injected with organoids with the single mutation (Fig.21). H&E staining of these tumours has been described by the pathologist (Prof. Vincenzo Canzonieri) as mucinous type low-grade adenocarcinoma. It is therefore possible to hypothesize that STARD3 promotes tumour transformation into cells where WNT pathway is activated. This hypothesis is partially supported by a recent article in which STARD3 inhibition blocks PI3K/AKT pathway in breast cancer[125] and another article in which its overexpression leads to PI3K/AKT activation in gastric cancer[94]. PI3K/AKT is often activated in adenoma carcinoma sequences after activation of the WNT pathway[8]. (Fig.2). To confirm this hypothesis in our set up, we performed Next Generation Sequencing (NGS) on organoids with the single

and double mutation. Unfortunately, due to high mycoplasma contamination and consequently low reads counts, the analysis did not produce any results and needs to be repeated in the future.

In order to evaluate STARD3 inhibition in a more physiological setting, we performed drug screening on colorectal cancer patient derived organoids. Patient derived organoid (PDO) recapitulate the primary tissues histopathological features, mutational landscape, and even responses to therapy.[118] Organoids were characterized by immunohistochemistry and the results in line with the literature showed maintenance expression markers (Fig.22) . Afterwards, organoids were treated with VS1. The results showed that some (five) patients responded to VS1 therapy by showing a similar or lower IC_{50} than the drugs currently used in the clinic (the first-line chemotherapy agent and regorafenib). FISH then allowed us to correlate the VS1 efficacy to STARD3 alteration levels, thus enabling us to support two further aspects of this research project: STARD3 as a potential target in colon cancer, at least in that subgroup of patients who exhibit STARD3 overexpression, and the efficacy of VS1 in protein inhibition. In the article already published by our group[82], the efficacy of the drug was evaluated on cell lines. For the first time here, its efficacy was demonstrated on organoids of patients, thus in a more physiological context close to clinical reality.

In conclusion, we identified STARD3 as a key player, which regulates different aspects of hallmark of cancer. Our hypothesis is that STARD3 is a valid therapeutic target for mCRC patients. This hypothesis is based on the following thesis results here summarized:

a) STARD3 is overexpressed in CRC tumors tissue compared to normal tissue and correlate with patient's survival.
b) Despite cancer cells contain complex genetic alterations, growth and survival can be affected by STARD3 single inactivation.

c) Inhibition of STARD3 (both with short hairpins and drugs) induces apoptosis in colorectal cancer cell lines and in a subset of patient derived organoids and inhibit tumor formation *in vivo*.

d) STARD3 overexpression transforms normal mouse colon organoids, inducing tumour formation in vivo (oncogene).

Whereas the mechanism of STARD3 is still elusive, from our results is interesting the role of this protein in colorectal cancer cells. Omics techniques (NGS, proteomic and lipidomic) will be used to dissect the role of STARD3 in colorectal cancer pathway. STARD3 inhibition, confirmed by shRNA and drug treatment, arise in a consistent reduction of cell viability and in an induction of apoptosis, suggesting an oncogene role of STARD3 in colorectal cancer. Further investigations are needed to understand in which way STARD3 acts, studying its role in cholesterol metabolisms. In fact, it is well demonstrated that alteration in cholesterol content is fundamental to the survival and growth of cancer cells as well as their ability to metastasize. For these reasons, STARD3 is an example of a new promising therapeutic target whose inhibition may provide benefits to colorectal cancer patients.

Bibliography

1. Jeught, K. V. der, Xu, H.-C., Li, Y.-J., Lu, X.-B. & Ji, G. Drug resistance and new therapies in colorectal cancer. *World J. Gastroenterol.* **24**, 3834–3848 (2018).
2. Schütte, M. *et al.* Molecular dissection of colorectal cancer in pre-clinical models identifies biomarkers predicting sensitivity to EGFR inhibitors. *Nat. Commun.* **8**, 14262 (2017).
3. Vacante, M., Borzì, A. M., Basile, F. & Biondi, A. Biomarkers in colorectal cancer: Current clinical utility and future perspectives. *World J. Clin. Cases* **6**, 869–881 (2018).
4. Fearon, E. R. Molecular genetics of colorectal cancer. *Annu. Rev. Pathol.* **6**, 479–507 (2011).
5. Nguyen, L. H., Goel, A. & Chung, D. C. Pathways of Colorectal Carcinogenesis. *Gastroenterology* **158**, 291–302 (2020).
6. Nakayama, M. & Oshima, M. Mutant p53 in colon cancer. *J. Mol. Cell Biol.* **11**, 267–276 (2019).
7. Driver mutations of the adenoma-carcinoma sequence govern the intestinal epithelial global translational capacity | PNAS. https://www.pnas.org/doi/10.1073/pnas.1912772117.
8. Pino, M. S. & Chung, D. C. THE CHROMOSOMAL INSTABILITY PATHWAY IN COLON CANCER. *Gastroenterology* **138**, 2059–2072 (2010).
9. Dinu, D. *et al.* Prognostic significance of KRAS gene mutations in colorectal cancer - preliminary study. *J. Med. Life* **7**, 581–587 (2014).
10. Li, X.-L., Zhou, J., Chen, Z.-R. & Chng, W.-J. p53 mutations in colorectal cancer-molecular pathogenesis and pharmacological reactivation. *World J. Gastroenterol. WJG* **21**, 84–93 (2015).
11. Vishwakarma, R. & McManus, K. J. Chromosome Instability; Implications in Cancer Development, Progression, and Clinical Outcomes. *Cancers* **12**, 824 (2020).
12. Satorres, C., García-Campos, M. & Bustamante-Balén, M. Molecular Features of the Serrated Pathway to Colorectal Cancer: Current Knowledge and Future Directions. *Gut Liver* **15**, 31–43 (2021).
13. De Palma, F. D. E. *et al.* The Molecular Hallmarks of the Serrated Pathway in Colorectal Cancer. *Cancers* **11**, 1017 (2019).
14. Minoo, P., Minoo, P. & Minoo, P. Toward a Molecular Classification of Colorectal Cancer: The Role of MGMT. *Front. Oncol.* **3**, (2013).
15. Renaud, F. *et al.* The serrated neoplasia pathway of colorectal tumors: Identification of MUC5AC hypomethylation as an early marker of polyps with malignant potential. *Int. J. Cancer* **138**, 1472–1481 (2016).
16. Serrated adenocarcinoma (SAC). https://www.pathologyoutlines.com/topic/colontumorserratedadeno.html.
17. Malki, A. *et al.* Molecular Mechanisms of Colon Cancer Progression and Metastasis: Recent Insights and Advancements. *Int. J. Mol. Sci.* **22**, 130 (2020).
18. Mezzapesa, M. *et al.* Serrated Colorectal Lesions: An Up-to-Date Review from Histological Pattern to Molecular Pathogenesis. *Int. J. Mol. Sci.* **23**, 4461 (2022).
19. Carethers, J. M. Microsatellite Instability Pathway and EMAST in Colorectal Cancer. *Curr. Colorectal Cancer Rep.* **13**, 73–80 (2017).
20. Pathology Outlines - Microsatellite instability pathway. https://www.pathologyoutlines.com/topic/colontumormolecularmicrosatellite.html.
21. Fondevila, F., Méndez-Blanco, C., Fernández-Palanca, P., González-Gallego, J. & Mauriz, J. L. Anti-tumoral activity of single and combined regorafenib treatments in

preclinical models of liver and gastrointestinal cancers. *Exp. Mol. Med.* **51**, 1–15 (2019).
22. Hideshima, T. *et al.* Discovery of selective small-molecule HDAC6 inhibitor for overcoming proteasome inhibitor resistance in multiple myeloma. *Proc. Natl. Acad. Sci.* **113**, 13162–13167 (2016).
23. Hoy, S. M. Sintilimab: First Global Approval. *Drugs* **79**, 341–346 (2019).
24. Hoelder, S., Clarke, P. A. & Workman, P. Discovery of small molecule cancer drugs: successes, challenges and opportunities. *Mol. Oncol.* **6**, 155–176 (2012).
25. Tripathy, D., Bardia, A. & Sellers, W. R. Ribociclib (LEE011): Mechanism of Action and Clinical Impact of This Selective Cyclin-Dependent Kinase 4/6 Inhibitor in Various Solid Tumors. *Clin. Cancer Res. Off. J. Am. Assoc. Cancer Res.* **23**, 3251–3262 (2017).
26. Tirumani, S. H. *et al.* Anti-VEGF molecular targeted therapies in common solid malignancies: comprehensive update for radiologists. *Radiogr. Rev. Publ. Radiol. Soc. N. Am. Inc* **35**, 455–474 (2015).
27. Balasubramaniam, S. *et al.* FDA Approval Summary: Rucaparib for the Treatment of Patients with Deleterious BRCA Mutation-Associated Advanced Ovarian Cancer. *Clin. Cancer Res. Off. J. Am. Assoc. Cancer Res.* **23**, 7165–7170 (2017).
28. Essel, K. G. & Moore, K. N. Niraparib for the treatment of ovarian cancer. *Expert Rev. Anticancer Ther.* **18**, 727–733 (2018).
29. Kuzu, O. F., Noory, M. A. & Robertson, G. P. The role of cholesterol in cancer. *Cancer Research* vol. 76 2063–2070 Preprint at https://doi.org/10.1158/0008-5472.CAN-15-2613 (2016).
30. Ding, X., Zhang, W., Li, S. & Yang, H. The role of cholesterol metabolism in cancer. *Am. J. Cancer Res.* **9**, 219–227 (2019).
31. Shafique, K. *et al.* Cholesterol and the risk of grade-specific prostate cancer incidence: evidence from two large prospective cohort studies with up to 37 years' follow up. *BMC Cancer* **12**, 25 (2012).
32. Allott, E. H. *et al.* Serum lipid profile and risk of prostate cancer recurrence: Results from the SEARCH database. *Cancer Epidemiol. Biomark. Prev. Publ. Am. Assoc. Cancer Res. Cosponsored Am. Soc. Prev. Oncol.* **23**, 2349–2356 (2014).
33. Disentangling the Association between Statins, Cholesterol, and Colorectal Cancer: A Nested Case-Control Study | PLOS Medicine. https://journals.plos.org/plosmedicine/article?id=10.1371/journal.pmed.1002007.
34. Wang, C. *et al.* Cholesterol Enhances Colorectal Cancer Progression via ROS Elevation and MAPK Signaling Pathway Activation. *Cell. Physiol. Biochem. Int. J. Exp. Cell. Physiol. Biochem. Pharmacol.* **42**, 729–742 (2017).
35. Lin, X. *et al.* Dietary Cholesterol Intake and Risk of Lung Cancer: A Meta-Analysis. *Nutrients* **10**, 185 (2018).
36. Lyu, Z. Y. *et al.* [Association between total cholesterol and risk of lung cancer incidence in men: a prospective cohort study]. *Zhonghua Liu Xing Bing Xue Za Zhi Zhonghua Liuxingbingxue Zazhi* **39**, 604–608 (2018).
37. Nelson, E. R. The significance of cholesterol and its metabolite, 27-hydroxycholesterol in breast cancer. *Mol. Cell. Endocrinol.* **466**, 73–80 (2018).
38. Touvier, M. *et al.* Cholesterol and breast cancer risk: a systematic review and meta-analysis of prospective studies. *Br. J. Nutr.* **114**, 347–357 (2015).
39. Statin Use and Breast Cancer Survival: A Nationwide Cohort Study from Finland | PLOS ONE. https://journals.plos.org/plosone/article?id=10.1371/journal.pone.0110231.
40. Jacobs, E. J., Newton, C. C., Thun, M. J. & Gapstur, S. M. Long-term use of cholesterol-lowering drugs and cancer incidence in a large United States cohort. *Cancer Res.* **71**, 1763–1771 (2011).
41. Cardwell, C. R., Hicks, B. M., Hughes, C. & Murray, L. J. Statin use after colorectal

cancer diagnosis and survival: a population-based cohort study. *J. Clin. Oncol. Off. J. Am. Soc. Clin. Oncol.* **32**, 3177–3183 (2014).
42. Freed-Pastor, W. A. *et al.* Mutant p53 disrupts mammary tissue architecture via the mevalonate pathway. *Cell* **148**, 244–258 (2012).
43. Staubach, S. & Hanisch, F.-G. Lipid rafts: signaling and sorting platforms of cells and their roles in cancer. *Expert Rev. Proteomics* **8**, 263–277 (2011).
44. Porstmann, T. *et al.* SREBP activity is regulated by mTORC1 and contributes to Akt-dependent cell growth. *Cell Metab.* **8**, 224–236 (2008).
45. Metabolomic Characterization of Human Prostate Cancer Bone Metastases Reveals Increased Levels of Cholesterol | PLOS ONE. https://journals.plos.org/plosone/article?id=10.1371/journal.pone.0014175.
46. Yue, S. *et al.* Cholesteryl ester accumulation induced by PTEN loss and PI3K/AKT activation underlies human prostate cancer aggressiveness. *Cell Metab.* **19**, 393–406 (2014).
47. Huang, P. *et al.* Cellular Cholesterol Directly Activates Smoothened in Hedgehog Signaling. *Cell* **166**, 1176-1187.e14 (2016).
48. Vaquero, J., Nguyen Ho-Bouldoires, T. H., Clapéron, A. & Fouassier, L. Role of the PDZ-scaffold protein NHERF1/EBP50 in cancer biology: from signaling regulation to clinical relevance. *Oncogene* **36**, 3067–3079 (2017).
49. Krause, M. R. & Regen, S. L. The structural role of cholesterol in cell membranes: from condensed bilayers to lipid rafts. *Acc. Chem. Res.* **47**, 3512–3521 (2014).
50. Maxfield, F. R. & van Meer, G. Cholesterol, the central lipid of mammalian cells. *Curr. Opin. Cell Biol.* **22**, 422–429 (2010).
51. Goldstein, J. L. & Brown, M. S. The LDL receptor. *Arterioscler. Thromb. Vasc. Biol.* **29**, 431–438 (2009).
52. Nguyen, M. K. L. *et al.* Linking Late Endosomal Cholesterol with Cancer Progression and Anticancer Drug Resistance. *Int. J. Mol. Sci.* **23**, 7206 (2022).
53. Hao, M. *et al.* Vesicular and non-vesicular sterol transport in living cells. The endocytic recycling compartment is a major sterol storage organelle. *J. Biol. Chem.* **277**, 609–617 (2002).
54. Iaea, D. B. & Maxfield, F. R. Cholesterol trafficking and distribution. *Essays Biochem.* **57**, 43–55 (2015).
55. Prinz, W. A. Non-vesicular sterol transport in cells. *Prog. Lipid Res.* **46**, 297–314 (2007).
56. Iaea, D. B., Mao, S. & Maxfield, F. R. Steroidogenic Acute Regulatory Protein-related Lipid Transfer (START) Proteins in Non-vesicular Cholesterol Transport. in *Cholesterol Transporters of the START Domain Protein Family in Health and Disease* (eds. Clark, B. J. & Stocco, D. M.) 173–188 (Springer New York, 2014). doi:10.1007/978-1-4939-1112-7_8.
57. D'Angelo, G., Vicinanza, M. & De Matteis, M. A. Lipid-transfer proteins in biosynthetic pathways. *Curr. Opin. Cell Biol.* **20**, 360–370 (2008).
58. Chimento, A. *et al.* Cholesterol and Its Metabolites in Tumor Growth: Therapeutic Potential of Statins in Cancer Treatment. *Front. Endocrinol.* **9**, 807 (2018).
59. Levin-Gromiko, U. *et al.* Amplified lipid rafts of malignant cells constitute a target for inhibition of aberrantly active NFAT and melanoma tumor growth by the aminobisphosphonate zoledronic acid. *Carcinogenesis* **35**, 2555–2566 (2014).
60. Currie, E., Schulze, A., Zechner, R., Walther, T. C. & Farese, R. V. Cellular fatty acid metabolism and cancer. *Cell Metab.* **18**, 153–161 (2013).
61. Ward, P. S. & Thompson, C. B. Metabolic reprogramming: a cancer hallmark even warburg did not anticipate. *Cancer Cell* **21**, 297–308 (2012).
62. Cairns, R. A., Harris, I., McCracken, S. & Mak, T. W. Cancer cell metabolism. *Cold Spring Harb. Symp. Quant. Biol.* **76**, 299–311 (2011).

63. Mollinedo, F. & Gajate, C. Lipid rafts as signaling hubs in cancer cell survival/death and invasion: implications in tumor progression and therapy: Thematic Review Series: Biology of Lipid Rafts. *J. Lipid Res.* **61**, 611–635 (2020).
64. Mollinedo, F. & Gajate, C. Lipid rafts as major platforms for signaling regulation in cancer. *Adv. Biol. Regul.* **57**, 130–146 (2015).
65. Murai, T. Cholesterol lowering: role in cancer prevention and treatment. *Biol. Chem.* **396**, 1–11 (2015).
66. Li, Y. C., Park, M. J., Ye, S.-K., Kim, C.-W. & Kim, Y.-N. Elevated levels of cholesterol-rich lipid rafts in cancer cells are correlated with apoptosis sensitivity induced by cholesterol-depleting agents. *Am. J. Pathol.* **168**, 1107–1118; quiz 1404–1405 (2006).
67. Zhuang, L., Kim, J., Adam, R. M., Solomon, K. R. & Freeman, M. R. Cholesterol targeting alters lipid raft composition and cell survival in prostate cancer cells and xenografts. *J. Clin. Invest.* **115**, 959–968 (2005).
68. Badana, A. K. *et al.* Lipid rafts disruption induces apoptosis by attenuating expression of LRP6 and survivin in triple negative breast cancer. *Biomed. Pharmacother. Biomedecine Pharmacother.* **97**, 359–368 (2018).
69. Raghu, H. *et al.* Localization of uPAR and MMP-9 in lipid rafts is critical for migration, invasion and angiogenesis in human breast cancer cells. *BMC Cancer* **10**, 647 (2010).
70. Amemiya-Kudo, M. *et al.* Transcriptional activities of nuclear SREBP-1a, -1c, and -2 to different target promoters of lipogenic and cholesterogenic genes. *J. Lipid Res.* **43**, 1220–1235 (2002).
71. Yang, T. *et al.* Crucial step in cholesterol homeostasis: sterols promote binding of SCAP to INSIG-1, a membrane protein that facilitates retention of SREBPs in ER. *Cell* **110**, 489–500 (2002).
72. Wüstner, D. & Solanko, K. How cholesterol interacts with proteins and lipids during its intracellular transport. *Biochim. Biophys. Acta BBA - Biomembr.* **1848**, 1908–1926 (2015).
73. Sun, L.-P., Li, L., Goldstein, J. L. & Brown, M. S. Insig Required for Sterol-mediated Inhibition of Scap/SREBP Binding to COPII Proteins in Vitro*♦. *J. Biol. Chem.* **280**, 26483–26490 (2005).
74. Nemecz, G. & Schroeder, F. Selective binding of cholesterol by recombinant fatty acid binding proteins. *J. Biol. Chem.* **266**, 17180–17186 (1991).
75. Raychaudhuri, S. & Prinz, W. A. The diverse functions of oxysterol-binding proteins. *Annu. Rev. Cell Dev. Biol.* **26**, 157–177 (2010).
76. Movement of accessible plasma membrane cholesterol by the GRAMD1 lipid transfer protein complex | eLife. https://elifesciences.org/articles/51401.
77. Enrich, C., Rentero, C., Grewal, T., Futter, C. E. & Eden, E. R. Cholesterol Overload: Contact Sites to the Rescue! *Contact Thousand Oaks Ventura Cty. Calif* **2**, 2515256419893507 (2019).
78. Storch, J. & Xu, Z. Niemann-Pick C2 (NPC2) and intracellular cholesterol trafficking. *Biochim. Biophys. Acta* **1791**, 671–678 (2009).
79. Mesmin, B., Antonny, B. & Drin, G. Insights into the mechanisms of sterol transport between organelles. *Cell. Mol. Life Sci. CMLS* **70**, 3405–3421 (2013).
80. Clark, B. J. The mammalian START domain protein family in lipid transport in health and disease. *J. Endocrinol.* **212**, 257–275 (2012).
81. Soccio, R. E. *et al.* The cholesterol-regulated StarD4 gene encodes a StAR-related lipid transfer protein with two closely related homologues, StarD5 and StarD6. *Proc. Natl. Acad. Sci.* **99**, 6943–6948 (2002).
82. Lapillo, M. *et al.* First-of-its-kind STARD3 Inhibitor: In Silico Identification and Biological Evaluation as Anticancer Agent. *ACS Med. Chem. Lett.* **10**, 475–480 (2019).

83. Vassilev, B. *et al.* Elevated Levels of StAR-Related Lipid Transfer Protein 3 Alter Cholesterol Balance and Adhesiveness of Breast Cancer Cells. *Am. J. Pathol.* **185**, 987–1000 (2015).
84. Stigliano, A. *et al.* Increased metastatic lymph node 64 and CYP17 expression are associated with high stage prostate cancer. *J. Endocrinol.* **194**, 55–61 (2007).
85. Alpy, F. *et al.* Metastatic lymph node 64 (MLN64), a gene overexpressed in breast cancers, is regulated by Sp/KLF transcription factors. *Oncogene* **22**, 3770–3780 (2003).
86. Zhang, M. *et al.* MLN64 mediates mobilization of lysosomal cholesterol to steroidogenic mitochondria. *J. Biol. Chem.* **277**, 33300–33310 (2002).
87. Charman, M., Kennedy, B. E., Osborne, N. & Karten, B. MLN64 mediates egress of cholesterol from endosomes to mitochondria in the absence of functional Niemann-Pick Type C1 protein. *J. Lipid Res.* **51**, 1023–1034 (2010).
88. Balboa, E. *et al.* MLN64 induces mitochondrial dysfunction associated with increased mitochondrial cholesterol content. *Redox Biol.* **12**, 274–284 (2017).
89. Montero, J. *et al.* Mitochondrial cholesterol contributes to chemotherapy resistance in hepatocellular carcinoma. *Cancer Res.* **68**, 5246–5256 (2008).
90. Cai, W., Ye, L., Sun, J., Mansel, R. E. & Jiang, W. G. Expression of MLN64 influences cellular matrix adhesion of breast cancer cells, the role for focal adhesion kinase. *Int. J. Mol. Med.* **25**, 573–580 (2010).
91. Sahlberg, K. K. *et al.* The HER2 amplicon includes several genes required for the growth and survival of HER2 positive breast cancer cells. *Mol. Oncol.* **7**, 392–401 (2013).
92. Fararjeh, A. F. S., Al Khader, A., Kaddumi, E., Obeidat, M. & AL-Fawares, O. Differential Expression and Prognostic Significance of STARD3 Gene in Breast Carcinoma. *Int. J. Mol. Cell. Med.* **10**, 34–41 (2021).
93. Qi, F., Qin, W.-X. & Zang, Y.-S. Molecular mechanism of triple-negative breast cancer-associated BRCA1 and the identification of signaling pathways. *Oncol. Lett.* **17**, 2905–2914 (2019).
94. Yun, S. M. *et al.* PPP1R1B-STARD3 chimeric fusion transcript in human gastric cancer promotes tumorigenesis through activation of PI3K/AKT signaling. *Oncogene* **33**, 5341–5347 (2014).
95. Qiu, Y. *et al.* Association analysis of ERBB2 amplicon genetic polymorphisms and STARD3 expression with risk of gastric cancer in the Chinese population. *Gene* **535**, 225–232 (2014).
96. Peretti, D., Kim, S., Tufi, R. & Lev, S. Lipid Transfer Proteins and Membrane Contact Sites in Human Cancer. *Front. Cell Dev. Biol.* **7**, 371 (2020).
97. Wilhelm, L. P. *et al.* STARD3 mediates endoplasmic reticulum-to-endosome cholesterol transport at membrane contact sites. *EMBO J.* **36**, 1412–1433 (2017).
98. Alpy, F. *et al.* STARD3 or STARD3NL and VAP form a novel molecular tether between late endosomes and the ER. *J. Cell Sci.* **126**, 5500–5512 (2013).
99. Di Mattia, T. *et al.* FFAT motif phosphorylation controls formation and lipid transfer function of inter-organelle contacts. *EMBO J.* **39**, e104369 (2020).
100. Kaiser, S. E. *et al.* Structural basis of FFAT motif-mediated ER targeting. *Struct. Lond. Engl. 1993* **13**, 1035–1045 (2005).
101. Loewen, C. J. R. & Levine, T. P. A highly conserved binding site in vesicle-associated membrane protein-associated protein (VAP) for the FFAT motif of lipid-binding proteins. *J. Biol. Chem.* **280**, 14097–14104 (2005).
102. Amarilio, R., Ramachandran, S., Sabanay, H. & Lev, S. Differential regulation of endoplasmic reticulum structure through VAP-Nir protein interaction. *J. Biol. Chem.* **280**, 5934–5944 (2005).
103. Hayashi, T., Rizzuto, R., Hajnoczky, G. & Su, T.-P. MAM: more than just a

housekeeper. *Trends Cell Biol.* **19**, 81–88 (2009).
104. STARD3/MLN64 is Striving at Membrane Contact Sites: Intracellular Cholesterol Trafficking for Steroidogenesis in Human Placental Cells :: Science Publishing Group. https://www.sciencepublishinggroup.com/journal/paperinfo?journalid=118&doi=10.11648/j.ajls.s.2015030302.19.
105. Di Mattia, T. *et al.* Identification of MOSPD2, a novel scaffold for endoplasmic reticulum membrane contact sites. *EMBO Rep.* **19**, e45453 (2018).
106. Höglinger, D. *et al.* NPC1 regulates ER contacts with endocytic organelles to mediate cholesterol egress. *Nat. Commun.* **10**, 4276 (2019).
107. UniProt Consortium. UniProt: a worldwide hub of protein knowledge. *Nucleic Acids Res.* **47**, D506–D515 (2019).
108. Tuccinardi, T., Manetti, F., Schenone, S., Martinelli, A. & Botta, M. Construction and Validation of a RET TK Catalytic Domain by Homology Modeling. *J. Chem. Inf. Model.* **47**, 644–655 (2007).
109. Lee, J., Freddolino, P. L. & Zhang, Y. Ab Initio Protein Structure Prediction. in *From Protein Structure to Function with Bioinformatics* (ed. J. Rigden, D.) 3–35 (Springer Netherlands, 2017). doi:10.1007/978-94-024-1069-3_1.
110. Give lipids a START: the StAR-related lipid transfer (START) domain in mammals | Journal of Cell Science | The Company of Biologists. https://journals.biologists.com/jcs/article/118/13/2791/28294/Give-lipids-a-START-the-StAR-related-lipid.
111. Hulce, J. J., Cognetta, A. B., Niphakis, M. J., Tully, S. E. & Cravatt, B. F. Proteome-wide mapping of cholesterol-interacting proteins in mammalian cells. *Nat. Methods* **10**, 259–264 (2013).
112. Horvath, M. P. *et al.* Structure of the lutein-binding domain of human StARD3 at 1.74 Å resolution and model of a complex with lutein. *Acta Crystallogr. Sect. F Struct. Biol. Commun.* **72**, 609–618 (2016).
113. Tsujishita, Y. & Hurley, J. H. Structure and lipid transport mechanism of a StAR-related domain. *Nat. Struct. Biol.* **7**, 408–414 (2000).
114. Reitz, J., Gehrig-Burger, K., Strauss III, J. F. & Gimpl, G. Cholesterol interaction with the related steroidogenic acute regulatory lipid-transfer (START) domains of StAR (STARD1) and MLN64 (STARD3). *FEBS J.* **275**, 1790–1802 (2008).
115. Drost, J. & Clevers, H. Organoids in cancer research. *Nat. Rev. Cancer* **18**, 407–418 (2018).
116. Drost, J. *et al.* Sequential cancer mutations in cultured human intestinal stem cells. *Nature* **521**, 43–47 (2015).
117. Matano, M. *et al.* Modeling colorectal cancer using CRISPR-Cas9–mediated engineering of human intestinal organoids. *Nat. Med.* **21**, 256–262 (2015).
118. Wensink, G. E. *et al.* Patient-derived organoids as a predictive biomarker for treatment response in cancer patients. *Npj Precis. Oncol.* **5**, 1–13 (2021).
119. Ooft, S. N. *et al.* Patient-derived organoids can predict response to chemotherapy in metastatic colorectal cancer patients. *Sci. Transl. Med.* **11**, eaay2574 (2019).
120. Moon, C., VanDussen, K. L., Miyoshi, H. & Stappenbeck, T. S. Development of a primary mouse intestinal epithelial cell monolayer culture system to evaluate factors that modulate IgA transcytosis. *Mucosal Immunol.* **7**, 818–828 (2014).
121. Schneider, C. A., Rasband, W. S. & Eliceiri, K. W. NIH Image to ImageJ: 25 years of image analysis. *Nat. Methods* **9**, 671–675 (2012).
122. Codrich, M. *et al.* Integrated multi-omics analyses on patient-derived CRC organoids highlight altered molecular pathways in colorectal cancer progression involving PTEN. *J. Exp. Clin. Cancer Res.* **40**, 198 (2021).

123. Borowicz, S. *et al.* The soft agar colony formation assay. *J. Vis. Exp. JoVE* e51998 (2014) doi:10.3791/51998.
124. Wang, Y., Liu, C. & Hu, L. Cholesterol regulates cell proliferation and apoptosis of colorectal cancer by modulating miR-33a-PIM3 pathway. *Biochem. Biophys. Res. Commun.* **511**, 685–692 (2019).
125. Li, P., Zhang, Z., Lv, H. & Sun, P. Inhibiting the expression of STARD3 induced apoptosis via the inactivation of PI3K/AKT/mTOR pathway on ER^+ breast cancer. *Tissue Cell* **79**, 101971 (2022).